Material characterisation for the modelling of the vacuum infusion process

Submitted in fulfilment of the requirements for the degree of Doctor of Engineering: Mechanical Engineering in the Faculty of Engineering at the Durban University of Technology

Mark Gilpin

April 2015

Supervisor: [redacted] Date: 2 SEPT 2015

Prof. David Jonson

Abstract

Vacuum Infusion (VI) and Resin Transfer Moulding (RTM) are liquid composite moulding processes used in the manufacture of components from composite materials. The composite material in this case consists of a resin matrix combined with fibre reinforcement. In both moulding processes, a dry reinforcement preform is placed in the mould cavity and a liquid resin is introduced, driven by a pressure differential. Two rigid surfaces are used in RTM to create a fixed mould cavity. In contrast VI implements only one rigid surface and a flexible membrane or vacuum bag to form a non rigid cavity. The flexible cavity in VI influences and differentiates resin flow behaviour from that of RTM. Modelling resin flow enables the velocity, pressure and flow direction to be predicted.

Resin flow in the RTM process is understood and modelled using Darcy's law. However, flow in the VI process is not accurately modelled due to the added complexity introduced as a result of the flexible cavity.

In the present work a novel approach was developed to investigate fluid flow in both processes. A unique experimental setup and testing procedure allowed for the direct comparison of fluid flow in RTM and VI. Identical flow parameters, conditions and preform construction were used in the assessment. The comparison isolated the effect of preform thickness variation as a differentiating factor influencing flow. From the experimentation, material behaviour was characterised and used to evaluate flow models for RTM and in particular VI. The model solutions were compared back to corresponding experiments. The pressure distribution behind the flow front, fill time and thickness behaviours were assessed.

The pressure distribution / profiles behind the flow front of both VI and RTM were noted to be scalable with flow front progression. The profiles were curved in the VI experiments and linear in the RTM case. All VI models evaluated including the non accumulation based model accurately predicted the pressure distribution and consequently thickness variations in the VI tests.

Fill times of the VI experiments were longer than that of the equivalent RTM tests. This behaviour is in contrast to previously interpreted fill time behaviour for the VI process based on VI models. It was also noted that the VI fill times were not only proportional to the square of the fill length, as in the RTM case, but also proportional to the square of the mass present. In addition, no significant accumulation was noted in the VI experiments.

Acknowledgements

I sincerely and thankfully acknowledge the following people, and company, who were instrumental in making this research possible:

My family for their support, understanding and encouragement.

Professor David Jonson for all the input, guidance and supervision.

My fellow postgraduate students and members of the Technology Station for their suggestions, assistance and camaraderie.

Denel Dynamics for the financial support and research funding.

Declaration

I declare that this thesis is my own unaided work except where due acknowledgement is made to others. This thesis is being submitted for the Degree of Doctor of Engineering to the Department of Mechanical Engineering at the Durban University of Technology, and has not been submitted previously for any other degree or examination

6/4/2015

Mark Gilpin Date

Contents

Abstract i

List of figures viii

Nomenclature x

1. Introduction 1

2. Literature review 4

2.1 Fibre reinforced polymer composites 4

2.2 Liquid composite moulding processes 5

2.2.1 Resin Transfer Moulding (RTM) 5

2.2.2 Vacuum Infusion (VI) 6

2.3 Fluid flow in porous media 8

2.3.1 The continuity equation 9

2.3.2 Permeability 11

2.4. Modelling of the fixed cavity RTM process 12

2.5 Modelling of the VI process 15

2.5.1 Accumulation based modelling 17

2.5.2 Non accumulation steady state model: 20

2.6 Preform compaction characterisation and modelling 22

2.7 Permeability characterisation and modelling 23

2.8. Summary 24

3 Experimentation 25

3.1 Testing equipment 25

3.1.1 Equipment components and instrumentation 27

3.2 Testing procedure 31

3.2.1 Injection fluid and injection pressure 33

3.2.2 Fabric preforms 33

3.2.3 Dry compacted thickness (VI) and cavity height (RTM) 34
3.2.4 Displacement and fluid pressure measurement 36
3.2.5 Fill time measurement 38
3.2.6 Fluid mass-time measurement 38
3.3 Experiments 40
3.3.1 Group1 – Multiple preforms 40
3.3.2 Group2 – Single preform 41
4. Experimental results 42
4.1 Group 1 – Multiple preforms 42
4.1.1 Saturated material response behaviour 43
4.1.2 Pressure distribution behind the flow front 47
4.1.3 Fill time results 48
4.2 Group 2 - Single preform 51
4.2.1 Experiment sets A and B 51
4.2.2 Experiment set C 53
4.3 Summary 55
5. Preform characterisation 57
5.1 Material characterisation – saturated expansion 57
5.2 Permeability characterisation 61
6. Evaluation of VI models 62
6.1 Input data 63
6.2 Solution method 63
7. Results of the VI models 65
7.1 Pressure profiles 65
7.2 Thickness variations 68
7.3 Fill time behaviour 70
7.4 Summary 80

8. Conclusion 81

References 85

Appendix A 89

Appendix B 95

List of figures

Figure 2. 1 – Resin Transfer Moulding (RTM) 6
Figure 2. 2 - Vacuum Infusion (VI) 6
Figure 2. 3 - Mass flow rates in a control volume 9
Figure 2. 4 - Pressure balancing in the VI process (Cross section) 15
Figure 2. 5 - Illustration of the non dimensional distance referential 18

Figure 3. 1 - VI (left) and RTM (right) setup configurations 25
Figure 3. 2 - Experimental setup (cross sectional schematic layout) 26
Figure 3. 3 - Rectilinear fluid flow and flow front propagation (video stills) 26
Figure 3. 4 - General layout of testing apparatus 29
Figure 3. 5 - Data acquisition hardware 29
Figure 3. 6 - LVDT support structure 30
Figure 3. 7 - Mounted pressure transmitters 30
Figure 3. 8 - Measurement of the dry compacted preform thickness (VI) 35
Figure 3. 9 - Measurement couple – LVDT and pressure transmitter 37
Figure 3. 10 - The LVDT's of the four measurement couples before infusion 38
Figure 3. 11 - Fibre glass fabrics 40

Figure 4. 1 - Pressure and surface displacement data recorded during a VI experiment 43
Figure 4. 2 - Measurement couple responses before inlet closure - Saturated expansion 44
Figure 4. 3 - Measurement couple responses after inlet closure: Saturated re-compaction 45
Figure 4. 4 – Measurement couple 1: Data from WR5 and WR5 – FRM experiments . 45
Figure 4. 5 - Pressure measurements at filled length of 200 mm (experiment set CSM) 47
Figure 4. 6 - Fill time results of the experimental sets performed in Group 1 48
Figure 4. 7 - Fill time results for WR5 and WR5-FRM vacuum infusion experiments . 49
Figure 4. 8 - Comparison of fill times between sets WR5 and WR10 50
Figure 4. 9 - Experiment set A 51
Figure 4. 10 - Experiment set A – Steady state 52

Figure 4. 11 - Experiment sets A and B 53
Figure 4. 12 - Experiment set C 54
Figure 4. 13 - Experimental set C – Steady state 54

Figure 5. 1 - Measurement couple 1 – experimental data for WR5 experiment 57
Figure 5. 2 - Compression response behaviour for WR5 – saturated expansion 58
Figure 5. 3 - Compression response behaviour for QA – saturated expansion 59
Figure 5. 4 - Compression response behaviour for CSM – saturated expansion 59

Figure 7. 1 - CSM pressure profile solution 66
Figure 7. 2 - WR5 pressure profile solution 66
Figure 7. 3 - QA pressure profile solution 67
Figure 7. 4 - Comparison of thickness variation with experimental data (CSM) 68
Figure 7. 5 - Comparison of thickness variation with experimental data (WR5) 69
Figure 7. 6 - Comparison of thickness variation with experimental data (QA) 69
Figure 7. 7 - CSM fill times 71
Figure 7. 8 - QA fill times 71
Figure 7. 9 - WR5 fill times 72
Figure 7. 10 - Permeability distribution of CSM experiment at filled length of 200 mm 75
Figure 7. 11 - Pressure profiles and inlet pressure gradients of WR5 experiments 76
Figure 7. 12 - Pressure profiles and inlet pressure gradients of CSM experiments 77
Figure 7. 13 - WR5 - inlet pressure gradient 78
Figure 7. 14 - CSM - inlet pressure gradient 78

Nomenclature

P_{comp}	-	Compaction pressure	(Pa)
P_{atm}	-	Atmospheric pressure	(Pa)
P	-	Fluid / resin pressure	(Pa)
V_f	-	Fibre volume fraction	(-)
n	-	number of layers	(-)
S_d	-	surface / areal / superficial density	(kg/m^2)
ρ	-	Density	(kg/m^3)
h	-	Preform thickness / cavity height	(m)
ϕ	-	Porosity	(-)
u	-	Darcy velocity	(m/s)
K	-	Permeability	(m^2)
μ	-	Viscosity	(Pa.s)
dP/dx	-	pressure gradient	(Pa/m)
V	-	Interstitial / filter fluid velocity	(m/s)
Q	-	Volumetric flow rate	(m^3/s)
$\mathring{m}$	-	Mass flow rate	(kg/s)
A_T	-	Total cross sectional area	(m^2)
A_R	-	Porous crosss sectional area	(m^2)
b	-	flow width	(m)
P_{in}	-	Inlet pressure	(Pa)

P_{out}	-	Outlet/flow front pressure	(Pa)
x_f	-	flow front position	(m)
t_f	-	filled length / flow front position	(s)
α	-	non dimensional position	(-)
L	-	filled length	(m)
h^*	-	thickness ratio	(-)
V_{f0}	-	fibre volume fraction at a P_{comp} = 1 Pa	(-)
B	-	Stiffing index	(-)
k_0	-	Kozeny constant	(m^2)
T	-	Temperature	(^oC)
δ	-	Surface displacement	(mm)

Subscripts:

RTM	-	Resin Transfer moulding
VI	-	Vacuum infusion

1. Introduction

Vacuum infusion (VI) and Resin transfer moulding (RTM) are liquid composite moulding processes. The processes share the same operating principle however the key difference is the formation of the mould cavity containing the preform reinforcement material. The RTM process implements a fixed cavity while the mould cavity in the VI process is flexible. The flexible cavity in VI influences and differentiates resin flow behaviour between the two processes. Modelling flow allows for flow behaviour to be predicted. The behaviour includes the direction, velocity and pressure of the flowing resin.

Resin flow in the RTM process is understood and is modelled using Darcy's law. The flow behaviour can be simulated using commercially available software. However, flow in the VI process is not accurately modelled due to the added complexity introduced as a result of the flexible cavity.

In order to interrogate fluid flow models it is necessary to compare the modelled behaviour with RTM and VI experiments. All models require specific properties unique to any particular fabric preform to be characterised. The RTM model requires a value of permeability to be determined while for VI models, permeability and thickness are both functions of compaction pressure which is related to the fluid pressure.

The novel contribution of the present work is the direct comparison of fluid flow in the RTM and VI processes under identical flow parameters and conditions. The comparison between the two processes isolates the effect of preform thickness variation as a contributing and differentiating factor influencing flow. Utilising the experimental setup, flow models for RTM and in particular VI, are evaluated against experiments. Through the unique setup and testing procedure, specific fabric preforms are tested under both VI and RTM conditions. From the experimentation, material and permeability characterisation is performed for a few particular preforms. The characterised behaviour is used to evaluate three VI models. The solutions of the flow models are compared back to the original corresponding VI experiments. The pressure distribution behind the flow front, fill time and thickness behaviours are compared. As a result of the direct experimental comparison between RTM and VI, insights are gained into aspects such as fluid accumulation, fill times and flow rates occurring in VI.

The study is presented with the following structure in line with the flow path of the research.

Chapter 2 describes fibre reinforced composite materials and the liquid composite moulding (LCM) methods of vacuum infusion (VI) and resin transfer moulding (RTM). As fluid flow in composite moulding is often characterised as flow through porous media, the continuity equation and Darcy's law are presented. The application of Darcy's law in the modelling of the RTM process is discussed with respect to fill times and pressure distribution behind the flow front. Three VI models are also reviewed. Two of the models are formulated through an accumulation based derivation. The third model is a proposed non accumulation steady state application of Darcy's law. Material and permeability characterisation and modelling of fabric preforms is also outlined in this chapter.

The experimental setup, equipment and testing procedures are described in Chapter 3. In addition, the comparative injection parameters under which the RTM and VI experiments are performed is also discussed. A description of how the parameters are established and measured is presented along with the method and equipment used to measure surface displacement and fluid pressure.

In Chapter 4 the experimental specimens are discussed. The experimentation is divided into two groups. Each group is comprised of experiment sets. Each set consists of one RTM and one VI experiment performed using the same fabric preform. The types of fabric reinforcement used in construction of the preforms and data specific to each of the experiment sets are presented.

The results of the experiment sets are presented in Chapter 5. The results are discussed in relation to the saturated material response, pressure profiles and fill times. A summary of observations and findings is discussed.

From the experimental work, three preforms and the related experiment sets are selected from which to evaluate the VI models. The solution models require unique data for each of the preforms to be determined. The data relates the thickness and permeability to the compaction or fluid pressure during filling. Chapter 6 outlines and highlights the method used in material and permeability characterisation and modelling.

In Chapter 7, the material and permeability models of the three preforms are implemented into three VI flow models. The solutions of the VI models are concluded in Chapter 8 with respect to the pressure profile, thickness variation and fill times. The results are compared to the initial and corresponding experiments.

2. Literature review

Vacuum Infusion (VI) and Resin Transfer Moulding (RTM) are closed mould liquid composite moulding methods. The methods are used to produce components from fibre reinforced polymer composite materials.

2.1 Fibre reinforced polymer composites

A fibre reinforced composite (FRC) is a material comprising two constituents. The material combines a polymer matrix with fibre reinforcement. The function of the fibre reinforcement in to bear the main load applied to the composite material, while the matrix mostly holds the fibres in position and distributes and transfers the load to the fibres. Components manufactured from FRC materials can be specifically designed to meet the loading requirements while also meeting design criteria of stiffness, strength, fatigue resistance and weight [1-3].

Fibre reinforcement can be natural or synthetic. In engineering applications the fibres are often made from glass, carbon or aramid while the fibre length can be short (discontinuous) or long (continuous). Continuous fibres can be grouped together to produce rovings or yarns. The rovings can then be woven with numerous weave patterns to produce fabrics. Short or chopped fibres are randomly orientated and held together using a binder or in some cases a carrier fabric [1]. Multiple layers of fibre reinforcement fabric are used to produce preforms used in liquid composite moulding processes [3].

Numerous polymer resins are used for the matrix in which the fibre reinforcement is contained. Polymeric matrix materials are generally categorised into two groups called thermosets and thermoplastics [3]. Thermoplastics are polymers which can be reshaped and reprocessed using heat and pressure. Thermoplastic composites have low moisture absorption good impact resistance and short processing times. In contrast thermoset composites do not soften when heated and cannot be reprocessed. This is due to cross linking of the polymer during curing. The highly cross linked structure results in poor fracture resistance of the composite [2]. However, thermoset composites possess better mechanical properties, durability, chemical resistance and thermal stability when

compared with thermoplastics. Examples of thermosets resins are epoxies, vinylesters and polyesters, all of which are used in liquid composite moulding processes [1].

2.2 Liquid composite moulding processes

Vacuum Infusion (VI) and Resin Transfer Moulding (RTM) are closed mould liquid composite moulding processes. Both processes involve the infusion of liquid resin into a dry fabric preform utilising a pressure gradient. For large components, closed moulding processes potentially offer higher production rates, lower production costs and increased quality when compared with open moulding processes such as hand lay-up. Closed moulding can also reduce operator exposure to harmful volatile organic compounds, such as styrene emissions [4].

RTM and VI are similar as both processes involve resin flow through porous media. However, a key difference is the method used to create the mould cavity containing the fabric preform.

2.2.1 Resin Transfer Moulding (RTM)

The Resin Transfer moulding process is used in the automotive, marine, aviation and consumer product markets to produce composite components. In RTM, two rigid tool surfaces are used to create a fixed cavity containing a dry fabric reinforcement preform. The thickness or height of the cavity remains constant during the introduction of liquid resin under pressure. The process can be performed using positive or vacuum pressures to create the driving pressure differential [2, 5]. Figure 2.1 illustrates the RTM process.

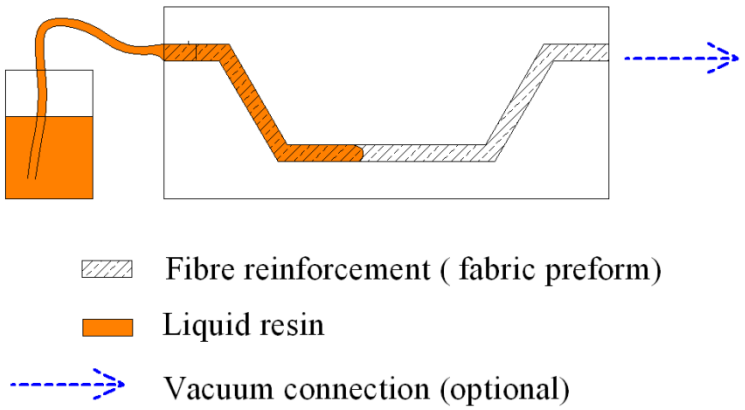

Figure 2. 1 – Resin Transfer Moulding (RTM)

2.2.2 Vacuum Infusion (VI)

Large composite components such as wind turbines and yachts can be produced using VI [6-8]. RTM is often limited to the manufacture of smaller components due to the higher cost of tooling. In contrast to RTM, VI utilises a flexible membrane or vacuum bag sealed to a rigid mould surface to form a mould cavity. Figure 2.2 illustrates the VI moulding process.The vacuum pressure performs two functions in the VI process. Firstly, the compaction of the fabric reinforcement within the mould cavity and secondly establishes the driving pressure differential for fluid flow.

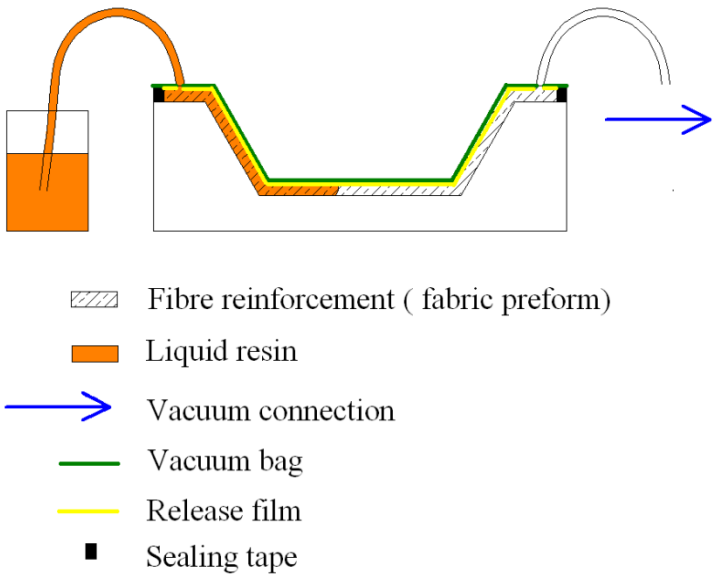

Figure 2. 2 - Vacuum Infusion (VI)

As resin flows into the mould cavity the flexible membrane allows the fabric preform thickness to vary as resin pressure changes during flow [9]. The variation in saturated thickness both influences and differentiates the flow behaviour when comparing the VI and RTM processes [10].

Vacuum infusion (VI), is also alternatively known as RIFT, VARTM, VM or SCRIMP^{TM} [11]. Williams et al. [12] provided a comprehensive review of many of the vacuum moulding techniques. Some techniques utilise highly permeable flow distribution media to promote resin flow and, in some cases, a semi-permeable membrane is used to control the flow. The high permeability flow distribution media is typically placed on top of the fabric preform and accelerates flow in the in-plane direction. The semi-permeable membrane is permeable to air and volatiles but not to resin. Venting through the membrane prevents excess resin from being removed from the system [13].

Throughout this work, VI refers to a vacuum infusion process without the use of distribution media or a semi permeable membrane. Correia et al. [11] noted that flow behaviour in RTM is comparable to VI if an incompressible preform is considered and no distribution media is employed.

2.3 Fluid flow in porous media

Flow through porous media was modelled by Henry Darcy in 1856. The work focused on the flow of water through porous soil [14] . The model (Eq.2.1) relates the local averaged or Darcy fluid velocity (u) to the pressure gradient (dP/dx). Here is the fluid viscosity and K is the permeability of the porous media. Permeability characterises the resistance of the porous media to fluid flow.

$$u = -\frac{K}{\mu}\frac{dP}{dx} \qquad (2.1)$$

The microscopic, filter or interstitial velocity (V) is related to the averaged fluid velocity (u) through Eq. 2.2, where ϕ is the porosity of the media.

$$V = \frac{u}{\phi} \qquad (2.2)$$

The interstitial velocity (V) can be written as

$$V = -\frac{K}{\mu\phi}\frac{dP}{dx} \qquad (2.3)$$

Flow rate (Q) can be determined by either multiplying the averaged fluid velocity (u) by the total cross sectional area (A_T) as in Eq. 2.4 or by multiplying the interstitial velocity (V) by the porous area (A_R) as in Eq. 2.5 [15].

$$Q = -\frac{K}{\mu}\frac{dP}{dx}A_T \qquad (2.4)$$

$$Q = -\frac{K}{\mu\phi}\frac{dP}{dx}A_R \qquad (2.5)$$

Darcy's law can only be applied to laminar flows at low Reynolds numbers. In addition, the fluid viscosity must also behave according to Newton's viscosity law [16]. Therefore fluid flow is governed predominantly by viscous and not inertia effects.

2.3.1 The continuity equation

The continuity equation expresses mass conservation through a fixed control volume [17, 18]. The continuity equation is presented here for two reasons. Firstly, as a clear explanation of the equation and secondly to show how the equation is manipulated into a form from which accumulation and non-accumulation based models are derived.

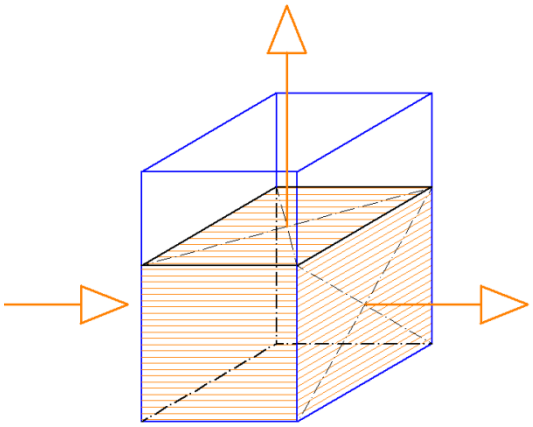

Figure 2. 3 - Mass flow rates in a control volume

Figure 2.3 illustrates a fixed control volume with fluid flow entering and leaving. If the inlet and outlet fluxes/flows are not equal then fluid accumulates within the control volume. This equates to a vertical surface displacement.

$$\oint_S \rho\, u\, \hat{n}\, dS + \frac{\partial}{\partial t} \oint_V \rho\, \phi\, dV = 0 \qquad (2.6)$$

Eq. 2.6, is the integral form of the continuity equation. The first term represents the surface integral of the fluxes entering and leaving the volume while the volume integral indicates flow accumulation. Eq. 2.7 illustrates the continuity equation in terms of the mass flow rates. The mass flow rates entering and leaving the control volume are the flux terms of the equation.

$$-\dot{m}_{\text{in}} + \dot{m}_{\text{out}} + \dot{m}_{\text{accumulation}} = 0 \qquad (2.7)$$

Mass flow rate ($\dot{m}$) can be expressed as the density of the fluid (ρ) multiplied by the volumetric flow rate (Q).

$$\dot{m} = \rho Q$$

The flow rate (Q) is equal to the fluid velocity (u) multiplied by the cross sectional area (A).

$$\mathring{m} = \rho u A$$

The cross sectional flow area (A) through which flow enters a control volume can be written in terms of height (h) and width (b) thus the mass flow rate can be written as

$$\mathring{m} = \rho u h b \qquad (2.8)$$

Eq. 2.9 expresses the mass flow rates (Eq. 2.7) of the continuity equation in partial differential form [19, 20].

$$-\rho u h b + \left(\rho u h b + \rho b \frac{\partial (uh)}{\partial x} \partial x\right) + \rho b \frac{\partial h}{\partial t} \partial x = 0 \qquad (2.9)$$

Simplifying Eq. 2.9 yields

$$\left(\rho b \frac{\partial (uh)}{\partial x} \partial x\right) + \rho b \frac{\partial h}{\partial t} \partial x = 0$$

If the fluid is incompressible, fluid density (ρ) remains constant

$$\left(b \frac{\partial (uh)}{\partial x} \partial x\right) + b \frac{\partial h}{\partial t} \partial x = 0$$

For rectilinear flow the width (b) of the volume element also remains constant.

$$\frac{\partial h}{\partial t} \partial x = \left(-\frac{\partial (uh)}{\partial x} \partial x\right)$$

The continuity equation (Eq. 2.6) can then be expressed as

$$\frac{\partial h}{\partial t} = -\frac{\partial (uh)}{\partial x} \qquad (2.10)$$

2.3.2 Permeability

Permeability is a characteristic of a fibre preform and is a measure of the resistance to fluid flow in a particular direction. Permeability can be determined from flow experiments performed either at a constant inlet inject pressure or at constant flow rate. The testing can be performed using a line or point feed configuration and permeability can be determined from transient or steady state flow [5].

For linear flow experiments under constant inlet injection pressure both transient and steady state conditions can be used to measure permeability (K). The equations are given by Eq. 2.12 and Eq. 2.11 respectively.

$$K = -\frac{Q\mu L}{A_T \Delta P} \qquad (2.11)$$

Equation 2.11 is implemented in measuring permeability in a steady state experiment. The equation is derived directly from Darcy's law (Eq. 2.4) by writing permeability as the subject of the formula. In the formulation, L is the filled length and ΔP is the pressure gradient established between inlet and outlet. A_T and μ are the cross sectional area of flow and the fluid viscosity respectively. Q is the established steady state flow rate [21].

$$K = \frac{\mu \phi x_f^2}{2\Delta P t_f} \qquad (2.12)$$

Equation 2.12 is use to derive permeability (K) from the observation of transient flow in line feed experiments [21, 22]. In the equation, ϕ and μ are the material porosity and fluid viscosity. ΔP is the constant pressure gradient established between the inlet and flow front during flow. The flow front position relative to the inlet is represented by x_f and the corresponding time taken to reach this position is identified as t_f .

2.4. Modelling of the fixed cavity RTM process

Fluid flow in the RTM process can be modelled using Darcy's law. The flow is assumed to be laminar, have no wall effects, and no flow in the through thickness direction. In addition, the resin is incompressible and the viscosity remains constant during flow. [23-25].

Darcy's law can be used to calculate fill time and pressure distribution behind the flow front. The pressure distribution or profile behind the flow front is determined through substitution of Darcy's law (Eq. 2.1) into the continuity equation (Eq. 2.10) and setting the accumulation term (dh/dt) equal to zero.

$$\frac{d}{dx}\left(\frac{Kh}{\mu}\frac{dP}{dx}\right) = 0 \qquad (2.13)$$

Noting that permeability (K) and cross sectional thickness (h) and do not change during the RTM process and assuming that the fluid viscosity (μ) remains constant. Then Eq. 2.13 can be reduced to Eq. 2.14

$$\frac{d^2P}{dx^2} = 0 \qquad (2.14)$$

Solving the differential equation using appropriate boundary conditions yields the pressure distribution (Eq. 2.16) between the inlet and flow front. [10, 22, 26-28].

Integrating Eq. 2.14 twice with respect to x yields Eq. 2.15. The equation contains two constants of integration c and d.

$$\int \frac{d^2P}{dx^2}\, dx = \int dx$$

$$\frac{dP}{dx} = c$$

$$\int \frac{dP}{dx}\, dx = \int c\, dx$$

$$P(x) = cx + d \qquad (2.15)$$

Constants c and d are solved using boundary conditions in the form of pressures at the inlet and flow front.

$P(0) = P_{in}$ (inlet pressure (P_{in}) at $x = 0$)

$P(L) = P_{out}$ (outlet pressure (P_{out}) at $x = L$)

Substitution of the boundary conditions in Eq. 2.15 yields

$$d = P_{in}$$

$$c = \frac{P_{out} - P_{in}}{L}$$

The pressure distribution behind the flow front in the RTM process is then given by Eq. 2.16. The pressure profile is linear and decreases from the inlet pressure to the pressure at the flow front.

$$P(x) = P_{in} + \left(\frac{P_{out} - P_{in}}{L}\right)x \qquad (2.16)$$

If the pressure at the flow front is set to zero ($P_{out} = 0$) then Eq. 2.16 reduces to Eq. 2.17.

$$P(x) = P_{in}\left(1 - \frac{x}{L}\right) \qquad (2.17)$$

The fill time or flow front propagation during RTM performed under constant pressure injection can be determined through a time integration of Darcy's law Eq. 2.3 and is given by Eq. 2.19 [21, 22, 29] .

$$V = \frac{K}{\mu\phi}\frac{dP}{dx}$$

Writing the velocity in differential form and integrating twice yields Eq. 2.19. First integrating with respect to time and secondly integrating with respect to distance yields Eq. 2.19.

$$\frac{dx}{dt} = \frac{K}{\mu\phi}\frac{dP}{dx} \qquad (2.18)$$

$$\int \frac{dx}{dt}\, dt = \frac{K}{\mu\phi}\frac{dP}{dx}\int dt$$

$$x_f = \frac{K}{\mu\phi}\frac{dP}{dx}\, t_f$$

$$\int x_f \, dx = \frac{K t_f}{\mu \phi} \int \frac{dP}{dx} dx$$

$$\frac{{x_f}^2}{2} = \frac{K t_f}{\mu \phi} \Delta P$$

$$t_f = \frac{\mu \phi x_f^2}{2 \Delta P K} \qquad (2.19)$$

Here t_f is the time taken to reach a particular filled distance (x_f). (ΔP) is the pressure difference between the inlet and flow front, μ is the viscosity of the resin. The porosity (ϕ) and permeability (K) are both characteristics of the fabric preform. Porosity of the fabric preform is determined form Eq. 2.22 after the fibre volume fraction is calculated using Eq. 2.21.

For rectilinear flow in the RTM process under constant pressure injection, the flow rate varies as the flow front progresses. However the flow rate at an instantaneous flow front position is constant through the filled length. This is a behavioural assumption required when Darcy's law is applied to model the RTM process.

2.5 Modelling of the VI process

In the VI process, pressure balancing between the fluid and preform fabric results in thickness variations occurring during flow. This is in contrast to the RTM process which implements a fixed cavity and as a result has no surface deflection or displacements.

The flexible nature of the mould cavity effects resin flow in the VI process. Dynamic thickness or cavity height variations occur as a result of pressure balancing between the fabric preform and the resin pressure [30]. The Terzaghi equation (Eq. 2.20) [15] is widely reported to describe the relationship [31, 32]. P_{comp} is the compaction pressure, while, P_{atm} and P are the atmospheric and resin pressures respectively.

$$P_{comp} = P_{atm} - P \qquad (2.20)$$

Figure 2.4 illustrates the pressure balancing in the VI process and the resulting thickness or cavity height variations (δh).

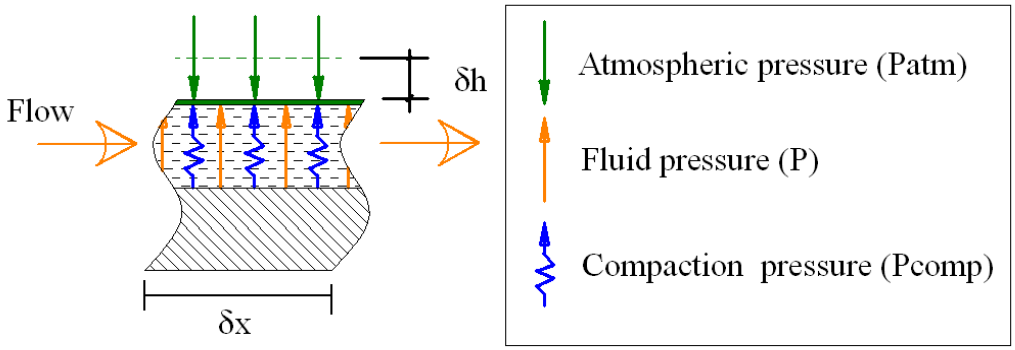

Figure 2. 4 - Pressure balancing in the VI process (Cross section)

There are three stages in the infusion process where compaction pressure applied to a fabric preform varies; pre-filling, filling and post-filling. In the "pre-filling" stage, the fabric preform undergoes dry compaction as vacuum is established. As resin is introduced during the "filling" stage, the resin pressure increases and reduces the compaction pressure. A reduction in compaction pressure allows for saturated relaxation or unloading of the preform. During the "post-filling" stage, the inlet is closed and

excess resin removed. The resin pressure gradients within the mould begin to equalize and compaction pressure is increased resulting in saturated re-compaction of the preform [33].

The thickness variations have been measured as surface displacement using LVDT's [13, 34, 35], laser [36, 37] and speckle photogrammetry [33] in VI experiments.

The thickness variations result in change to fibre volume fraction. The fibre volume fraction (V_f) is determined from (Eq. 2.21), where S_d is the areal/superficial density of the fabric, n is the number of layers in the preform, ρ is the density of the fibre material and h is the cavity height or preform thickness.

$$V_f = \frac{n\, S_d}{\rho h} \qquad (2.21)$$

Porosity of a given fabric is then determined from Eq. 2.22.

$$\phi = 1 - V_f \qquad (2.22)$$

The continuity equation models fluid flow in an expanding control volume. The approach indicates the direct relationship between thickness variation and fluid accumulation. However, if thickness variations are predominantly the result of pressure balancing and not directly accompanied by fluid accumulation then a non accumulation based model could be applicable. Presented here is an explanation of two accumulation based models used to model the VI process. The models are based on the continuity equation. A non-accumulation steady state model is also derived and presented.

2.5.1 Accumulation based modelling

The continuity equation has been used to model fluid flow in the VI process. Correia et al [10] consolidated many previously reported analytical models by numerous authors [30, 38-40]. It was shown that all the models were based on the continuity equation (Eq. 2.11) and individual differences were the result of simplifying assumptions. A consolidated VI model was then proposed. Modi [26] argued that the formulation of Correia's model considered constant flow rate and proposed an alternative formulation and model.

In the present work both the Correia [10] and Modi [26] models are compared with VI experiments. Both formulations share a common structure. Differences between the two models are highlighted in the formulations. Only key steps in the both formulations are presented here. Full detailed derivations are shown in Appendix A and B.

Both formulations apply Darcy's law (Eq. 2.1) to the continuity equation (Eq. 2.10) this yields Eq. 2.23

$$\frac{\partial h}{\partial t} = -\frac{\partial}{\partial x}\left(\frac{-Kh}{\mu}\frac{\partial P}{\partial x}\right) \tag{2.23}$$

However, permeability (K) and thickness (h) are both functions of pressure

Expanding Eq. 2.23 yields:

$$\frac{\partial h}{\partial t} = \frac{1}{\mu}\left[\left(h\frac{\partial K}{\partial P}\left(\frac{\partial P}{\partial x}\right)^2\right) + \left(K\frac{\partial h}{\partial P}\left(\frac{\partial P}{\partial x}\right)^2\right) + \left(Kh\frac{\partial^2 P}{\partial x^2}\right)\right] \tag{2.24}$$

Figure 2.5 illustrates the rectilinear fluid flow in VI process at two time periods during filling. The instantaneous flow front position (*ff*) varies for position 1 to 2. The thickness (h), pressure (P) and filled length (L) at each position is indicated. A fixed position along the mould cavity is illustrated by a dot marker.

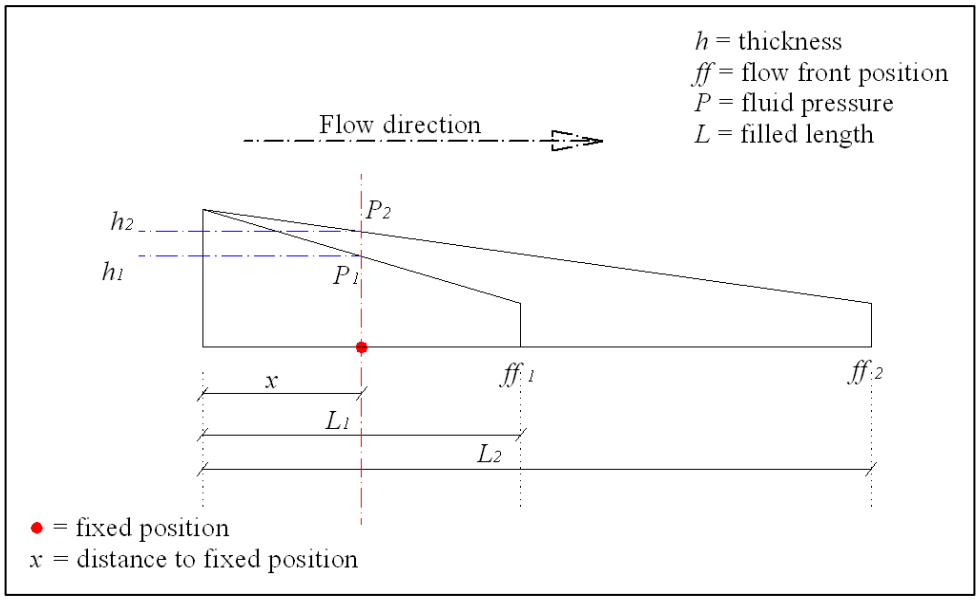

Figure 2. 5 - Illustration of the non dimensional distance referential

Correia and Modi [10, 26], noted the pressure profile solution to be scalable between the inlet and flow front and introduced a non dimensional parameter (α) (Eq. 2.25) which related a fixed position x to the filled length.

$$\alpha = \frac{x}{L} \qquad (2.25)$$

The inlet is positioned at $\alpha = 0$ while the flow front is located at $\alpha = 1$, this is regardless of the time. During flow front progression the pressure at a fixed point increases. However, the pressure at a non-dimensional position remains constant as the scalable pressure profile moves along with the flow front or filled length [10, 26].

Applying (Eq. 2.25) to (2. 24) yields:

$$\frac{\partial h}{\partial t} = \frac{Kh}{\mu L^2}\left[\left(\frac{1}{K}\frac{\partial K}{\partial P} + \frac{1}{h}\frac{\partial h}{\partial P}\right)\left(\frac{\partial P}{\partial \alpha}\right)^2 + \left(\frac{\partial^2 P}{\partial \alpha^2}\right)\right] \qquad (2.26)$$

Considering the LHS ($\partial h/\partial t$) of (Eq. 2.26) with reference to Figure 2.5, the change in thickness with time of a fixed position x is then a composite function (Eq. 2.27). As the flow front progresses or filled length increases with time ($\partial L/\partial t$), the non dimensional distance representing x changes ($\partial \alpha/\partial L$). In turn the pressure increases as the non-

dimensional distance changes ($\partial P/\partial \alpha$). The thickness then varies in relation to the pressure ($\partial h/\partial P$). The composite function is shown in Eq. 2.27.

$$\frac{\partial h}{\partial t} = \frac{\partial h}{\partial P}\frac{\partial P}{\partial \alpha}\frac{\partial \alpha}{\partial L}\frac{\partial L}{\partial t} \tag{2.27}$$

The formulations by Correia [10] and Modi [26] are identical to this point. The only difference between the two formulations is the way in which the change in filled length varies with time ($\partial L/\partial t$).

Correia et al [10] presented Eq.2.28 for the change in filled length with time or flow front propagation. Here h^* is the ratio of laminate thickness (h) to the thickness at the flow front ($h_{[\alpha=1]}$).

$$\frac{\partial L}{\partial t} = -\frac{Kh^*}{\mu}\frac{\partial P}{\partial \alpha}\frac{\partial \alpha}{\partial x} \tag{2.28}$$

where

$$h^* = \frac{h}{h_{[\alpha=1]}}$$

Modi [26] argued that the change in filled length with time should be expressed as Eq.2.29 where ϕ is the porosity of the preform reinforcement.

$$\frac{\partial L}{\partial t} = -\frac{K}{\mu\phi}\frac{\partial P}{\partial \alpha}\frac{\partial \alpha}{\partial L} \tag{2.29}$$

Substituting Eq. 2.28 and Eq. 2.29 into Eq. 2.27 and then into Eq. 2.26 yields the models proposed by Corriea and Modi, respectively. Corriea et al model is expressed in Eq. 2.30 while Modi's model is given by equation Eq. 2.31.

$$\frac{d^2P}{d\alpha^2} = -\left[\left(\frac{1-h^*\alpha}{h}\right)\frac{dh}{dP} + \left(\frac{1}{K}\right)\frac{dK}{dP}\right]\left(\frac{dP}{d\alpha}\right)^2 \tag{2.30}$$

$$\frac{d^2P}{d\alpha^2} = -\left[\left(\frac{\phi+\alpha^2}{h\phi}\right)\frac{dh}{dP} + \left(\frac{1}{K}\right)\frac{dK}{dP}\right]\left(\frac{dP}{d\alpha}\right)^2 \tag{2.31}$$

2.5.2 Non accumulation steady state model:

If the thickness variations in the VI process are not directly accompanied by fluid accumulation then VI like RTM could be modelled using Darcy's law applied to the non accumulation steady state continuity equation. The pressure driven thickness variations affect the permeability (K) and cross sectional area (A_T) of flow while a constant flow rate is established for an instantaneous filled length.

The non accumulation continuity equation is derived from Eq. 2.10 by setting the accumulation term equal to zero (Eq. 2.32).

$$0 = \frac{\partial(uh)}{\partial x} \qquad (2.32)$$

Applying Darcy's equation for flow rate (Q) (Eq. 2.4) into the continuity equation (Eq. 2.32) yields

$$0 = \frac{d}{dx}\left(-\frac{K}{\mu}\frac{dP}{dx}A_T\right) \qquad (2.33)$$

Where the cross sectional area of flow (A_T) is a product of width (b) and height (h)

$A_T = bh$

Substituting into (Eq. 2.33) yields

$$0 = -\frac{d}{dx}\left(\frac{Kbh}{\mu}\frac{dP}{dx}\right)$$

Noting that (b) remains constant during rectilinear flow and assuming fluid viscosity (μ) remains constant yields (Eq. 2.34).

$$0 = -\frac{b}{\mu}\frac{d}{dx}\left(Kh\frac{dP}{dx}\right)$$

$$0 = -\frac{d}{dx}\left(Kh\frac{dP}{dx}\right) \qquad (2.34)$$

Permeability (K) and thickness (h) are both functions of fluid pressure (P). Expanding (Eq. 2.34) and simplifying yields (Eq. 2.35).

$$0 = -\left(\frac{dK}{dP}\frac{dP}{dx}h\frac{dP}{dx}\right) - \left(K\frac{dh}{dP}\frac{dP}{dx}\frac{dP}{dx}\right) - \left(Kh\frac{dP}{dx}\frac{dx}{dP}\frac{dP}{dx}\right)$$

$$0 = -\left(h\frac{dK}{dP}\left(\frac{dP}{dx}\right)^2\right) - \left(K\frac{dh}{dP}\left(\frac{dP}{dx}\right)^2\right) - \left(Kh\frac{d^2P}{dx^2}\right)$$

Simplifying yields:

$$\frac{d^2P}{dx^2} = -\left[\left(\frac{1}{h}\right)\frac{dh}{dP} + \left(\frac{1}{K}\right)\frac{dK}{dP}\right]\left(\frac{dP}{dx}\right)^2 \qquad (2.35)$$

Equation (2.35) is the steady state non-accumulation based model for the VI process. The formulation acknowledges that the thickness and permeability are both functions of pressure however the instantaneous flow rate for a given filled length is constant throughout the filled region. This is the case in the modelling of the RTM process using Darcy's law.

2.6 Preform compaction characterisation and modelling

The changes in compaction pressure result in variations in thickness and therefore, fibre volume fraction. The relationship is the compression response behaviour of the fabric preform. The behaviour is rather complex and is effected by numerous factors, such as, the maximum magnitude, application rate and direction (loading or unloading) of the applied compaction pressure. Other factors include; the preform condition (dry or saturated), the number of layers, number of compaction cycles and compaction pressure history [26].

Preform compression response, has been modelled as nonlinear elastic [41, 42] behaviour and in some cases nonlinear viscoelastic behaviour is highlighted as significant [43-45]. Permanent deformation behaviour is also considered to affect the relationship between thickness and compaction pressure [46, 47].

Compression experiments are performed to determine the compression response behaviour. A popular method involves the compaction of a fabric preform between two rigid plates or surfaces [36, 39, 47-50]. Modi et al [27], suggested that reinforcement compliance behaviour measured utilising rigid tool surfaces may not accurately represent compaction pressure and thickness variations in the VI process. It was hypothesised that the differences in compaction events as well as surface contact may result in different compression response behaviour, which could lead to different empirical models.

Robitaille et al [51, 52] modelled compaction pressure (P_{comp}) and fibre volume fraction (V_f) changes using equation Eq. 2.36. The model is a power law containing two coefficients where V_{fo} is the fibre volume fraction at 1Pa compaction pressure and B is a stiffening index. Both coefficients are determined through fitting the model to experimental data [10].

$$V_f = V_{fo} {P_{comp}}^B \qquad (2.36)$$

2.7 Permeability characterisation and modelling

The thickness variations which occur in the VI process affect the fibre volume fraction/porosity of the fabric preform. Permeability is affected by the geometric properties of the porous media and is therefore influenced by changes in the fibre volume fraction. In order to apply Darcy's law to flow in fabric preforms it is necessary to establish the relationship between permeability and fibre volume fraction.

In 1927, Kozeny derived an analytical model for the flow through an array of channels of varying cross sections. Based on the model theory, the Kozeny-Carmen model was developed to model flow through porous media [53]. The Kozeny-Carmen equation (Eq.2.37) is widely noted to characterise the permeability and fibre volume fraction relationship for fibre preforms [22, 26, 40, 45, 54]. Here K is the reinforcement permeability, V_f is the volume fraction and k_0 is the Kozeny constant which is a empirical permeability coefficient estimated from permeability experimentation.

$$K = k_0 \frac{\left(1 - V_f\right)^3}{{V_f}^2} \quad (2.37)$$

Govignon et al [33, 49], used a modified Kozeny-Carmen (Eq. 2.38) to model the permeability fibre volume fraction relationship where C is a modified Kozeny constant. Kessels et al [36], performed experiments which measured permeability as a function of preform height/thickness. For the specific preforms used in this study it was found that permeability thickness relationship was best modelled using a power law.

$$K = C \frac{\left(1 - V_f\right)^{n+1}}{{V_f}^n} \quad (2.38)$$

2.8. Summary

In summary, chapter 2 describes fibre reinforced composite materials and the liquid composite moulding (LCM) methods of vacuum infusion (VI) and resin transfer moulding (RTM). As fluid flow in composite moulding is often characterised as flow through porous media, the continuity equation and Darcy's law are reviewed.

The application of Darcy's law in the modelling of the RTM process is discussed with respect to fill times and pressure distribution behind the flow front.

Pressure balancing in VI is the key feature influencing and differentiating flow from that of RTM. Three VI fluid flow models are discussed. Two of the models are formulated through an accumulation based derivation while a third model is a proposed non accumulation steady state application of Darcy's law. All models implement both the permeability and thickness variations as functions of compaction pressure. This behaviour is characterised through experimentation and is also discussed.

The aim of the research is to directly compare fluid flow in both RTM and VI under identical flow conditions and parameters. This isolates the effect of pressure balancing as the differentiating factor. Utilising experimental data the VI models are assessed and evaluated.

3 Experimentation

In line with the objective of the research an experimental setup was developed which enabled direct comparisons to be made between fluid flow in RTM and VI. The experiments were designed to measure the saturated material response behaviour which differentiates VI from RTM. In order to characterise each process, pressures and, in the case of the VI experiments, surface displacements, were measured at various locations whilst specific infusion parameters and conditions were maintained constant. The constant infusion parameters allowed for an appropriate reference condition to be defined. In this section the testing equipment, testing procedure and experimental groups are discussed.

3.1 Testing equipment

The experimentation used specially designed equipment, which could be configured for either line or point feed setups in both RTM and VI processes. Oil with an appropriate viscosity was used instead of resin to avoid problems associated with resin curing.

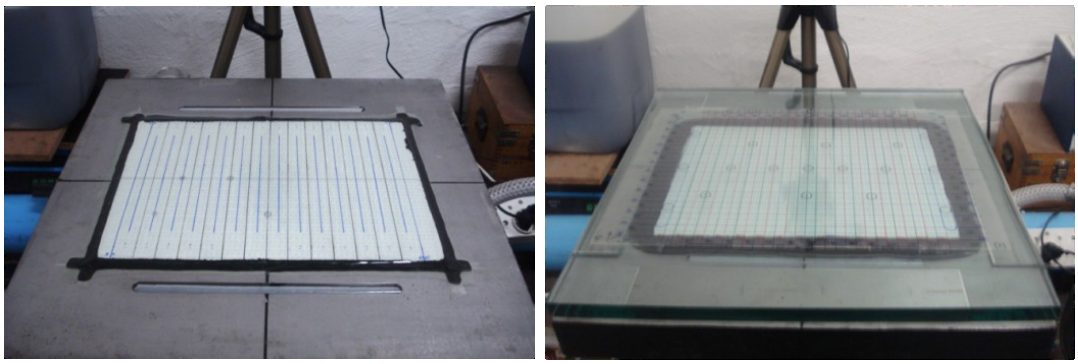

Figure 3. 1 - VI (left) and RTM (right) setup configurations

Figure 3.1 illustrates the experimental setup of both processes while Figure 3.2 shows a schematic cross sectional view. The figures illustrate the lower mould surface which was common to both processes. However, the mould cavity was formed using a vacuum bag in VI and a thick glass plate for RTM.

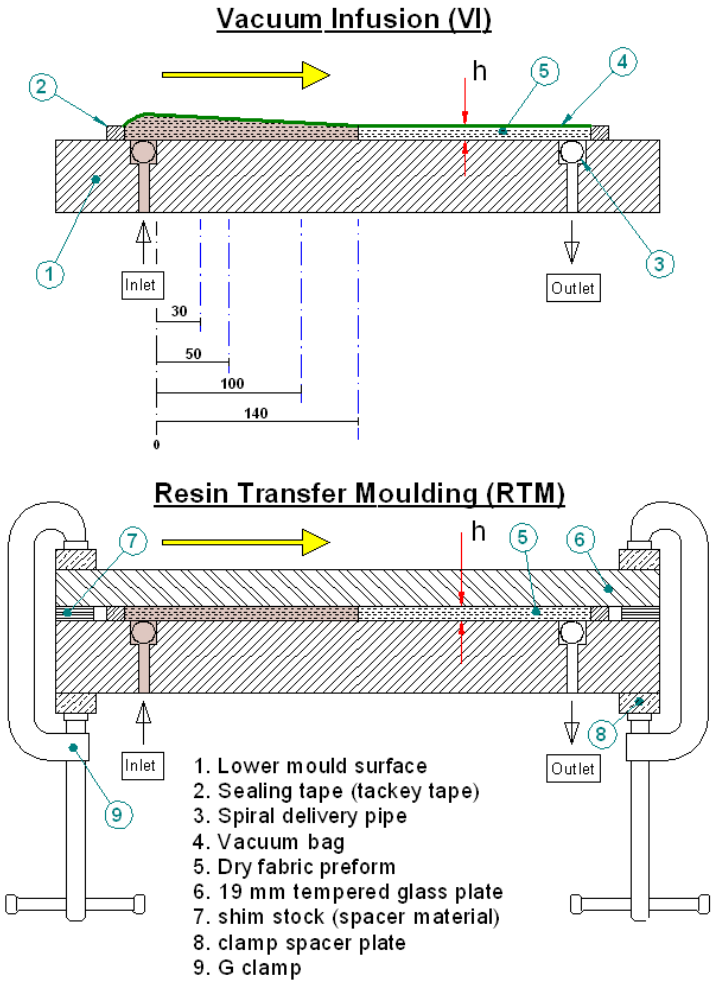

Figure 3. 2 - Experimental setup (cross sectional schematic layout)

Figure 3.3 illustrates the fluid flow between two channels at opposite ends of the lower mould surface. The inlet channel was connected to an oil reservoir and the outlet connected to a vacuum pump via an oil trap.

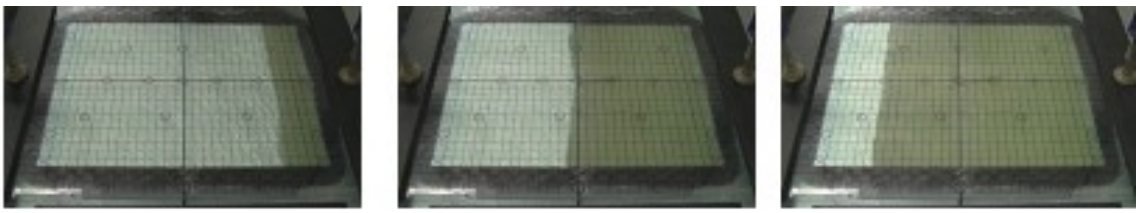

Figure 3. 3 - Rectilinear fluid flow and flow front propagation (video stills)

The differential pressure between the inlet and outlet channels thus drives the fluid flow during an experiment. The experimental setup allowed for test parameters and conditions to be measured for a comparison between the processes. Fill times were

recorded for both processes. In addition, fluid pressure and surface displacement were measured in the VI experiments.

3.1.1 Equipment components and instrumentation

The following is a numbered list of components and equipment utilized in the complete experimental apparatus. The numbers correspond to components indicated in Figures.3.4 - 3.7.

1. Lower mould surface – houses the inlet, vent ports and pressure transmitters.

   Manufactured form tool steel, machined and surface ground flat

2. Fluid/ oil trap – Allow flow to be maintained after flow reaches the vacuum port, The slopping side of the trap allows oil to be easily drained and reused.

3. Fluid reservoir containing infusion oil (*Engen Gencirc 150*)

4. Red handle valves utilized in point feed infusion. Double valve isolation.

5. Blue handle valves utilized for line feed infusion. Double valve isolation

6. *National Instruments*, SCXI Data acquisition system.

   6.1 NI SCXI-1600 Data acquisition and control module

   6.2 SCXI -1540 LVDT module and SCXI -1315 terminal block

   6.3 SCXI-1102B Signal conditioning module and SCXI -1308 Current input terminal block

7. *National Instruments Labview* software for data display and recording

8. Flat glass plate. Thickness – 19 mm used in RTM configuration

9. Displacement measurement apparatus

   9.1 LVDT support arm

   9.2 LVDT (D60500UL10- *RDP electronics*) Unguided armature/Stroke0-10mm.

10. Switch mode power supply 2222 (*PR Electronics*) Converts 230VAC to steady 24VDC. Power source for pressure transmitters

11. Pressure transducer (Wika instruments, model S10). Range: 0 – 2 Bar absolute; loop powered, 4-20 mA.

12. Vacuum pump: Gebr Becker vacuum pump. Capacity $70m^3/h$.

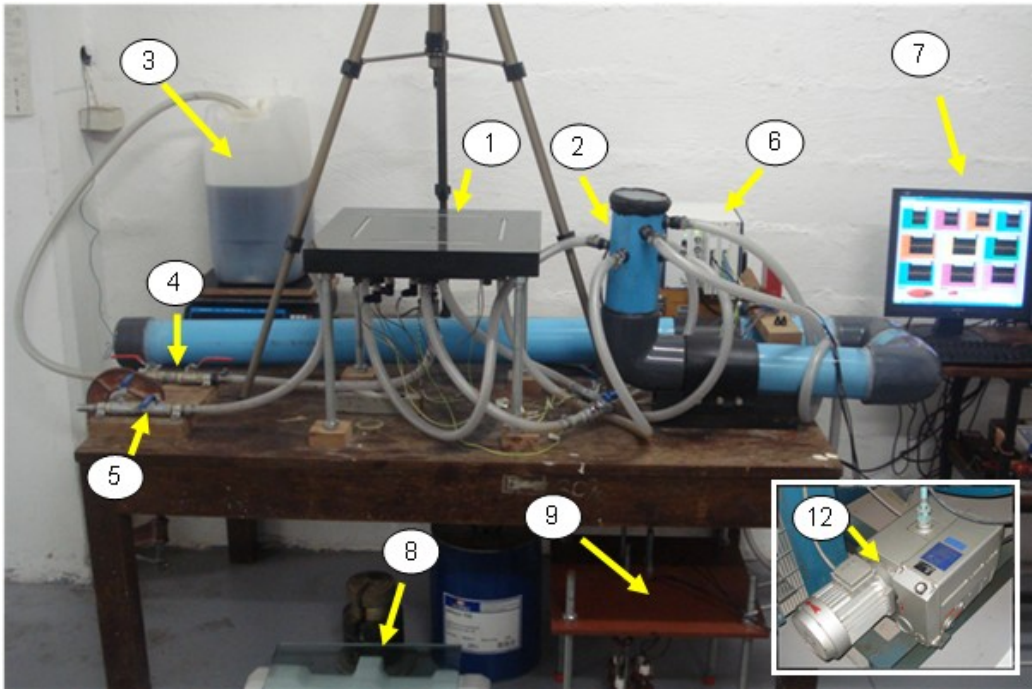

Figure 3. 4 - General layout of testing apparatus

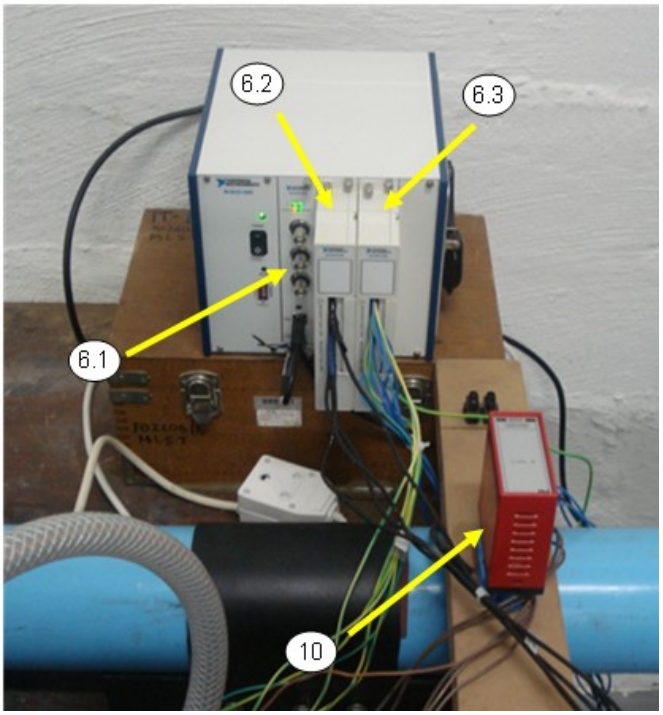

Figure 3. 5 - Data acquisition hardware

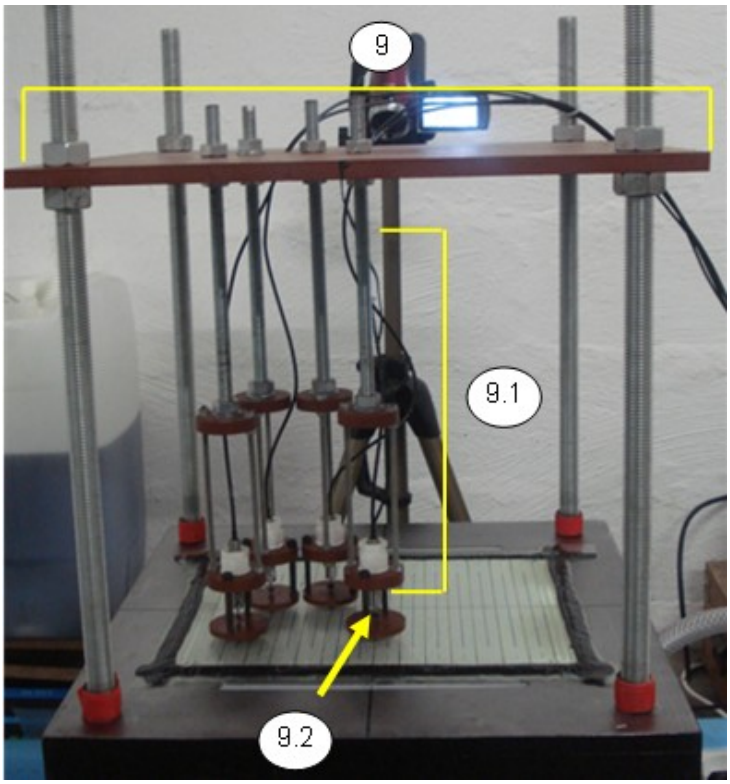

Figure 3. 6 - LVDT support structure

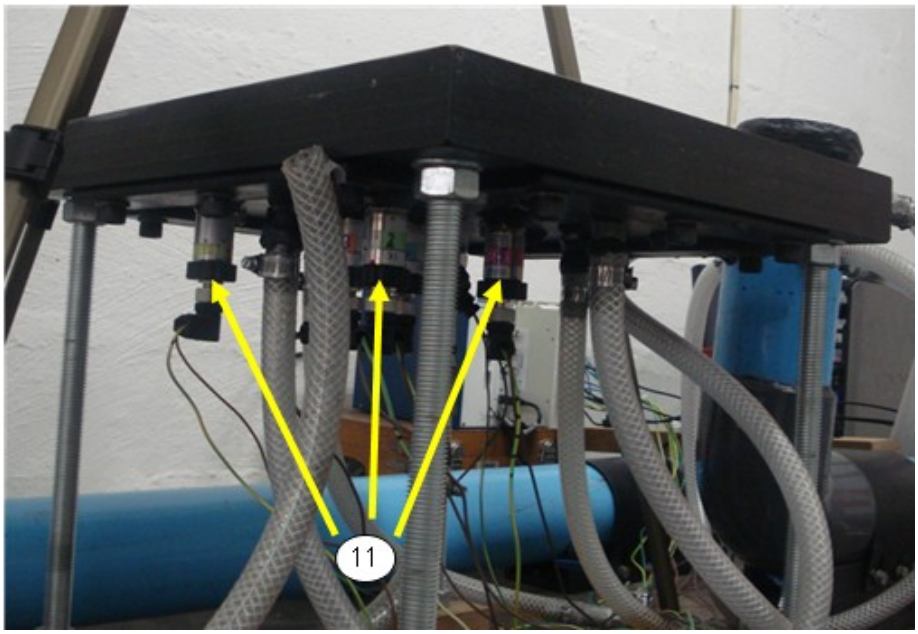

Figure 3. 7 - Mounted pressure transmitters

3.2 Testing procedure

In order to compare fluid flow in VI directly with that of RTM it was necessary to test the same preform under identical flow conditions and parameters. These comparative tests were performed in experiment sets. Each set consisted of one RTM and one VI experiment. The following highlights the general testing procedure followed and indicates how equivalency is obtained. The testing procedure is presented here in the sequential steps. Further details of specific aspects are presented in subsections 3.2.1 – 3.2.6. The subsections are indicated where applicable.

1. The VI and RTM tests for any given experiment set are performed on the same day, ensuring oil viscosity and injection pressure remain consistent. The daily atmospheric pressure, oil temperature and viscosity are recorded. (*Section 3.2.1*).

2. The VI experiment is performed first. A fabric is cut, staked and placed on the lower mould surface. A template is then placed over the preform stake and the fabric is cut to the exact dimensions of the mould between inlet and ountlet (*section 3.2.2*). Sealing tape (tackey tape) is applied to the periphery of the preform and a vacuum bag is placed over the top.

3. The inlet valves are secured and vacuum is established via the outlet channel and oil trap connected to a vacuum pump. Following a number of compaction cycles the preform compacted thickness is measured and recorded. This compacted thickness will later be matched in the comparative RTM test (*section 3.2.3*).

4. LVDT's are then placed over the compacted preform in contact with the vacuum bag. The displacement of the compacted surface is measured in this manner while the fluid pressure is measured with pressure transmitters. One LVDT and one pressure transmitter form a measurement couple. The measurement couple measures the dynamic relationship between fluid pressure and surface displacement during filling (*section 3.2.4*).

5. The inlet or feed pipe is then placed in the oil reservoir and video equipment is setup to record the flow front propagation during filling (*sections 3.2.5*). In some

experiments, fluid mass measurements were also recorded dynamically using the video footage (Section *3.2.6*).

6. At the start of the VI experiment three actions are performed simultaneously with the assistance of others. Firstly, the inlet value is opened allowing fluid flow to commence. Secondly, the video recording is started to capture flow front propagation. Thirdly, data logging from the measurement couples is initiated.

7. During the VI test, fluid propagates through the laminate leading to flow front advancement. Some VI tests are allowed to continue flowing once the mould cavity is full. These tests are performed to investigate steady state flow behaviour.

8. On completion of the VI experiment the mould surface is cleaned and all lines and channels are drained in preparation for the accompanying RTM test. In the same manner as the VI setup an identical preform is constructed on the lower mould surface. The cavity required by RTM is formed between the lower mould surface and a thick glass plate. This cavity height is fixed utilising shim stock.

9. The correct quantity of shim stock is applied to the surface of the lower mould in 4 locations surrounding the preform. The quantity and thickness of the shim stock is determined from the height measurement performed in the VI experiment (*Section 3.2.3*)

10. Sealing tape (tackey tape) is applied to the periphery of the preform. A 19 mm thick glass plate is placed over the preform and sealed.

11. After vacuum is established the identical start up procedure to that of the VI test is followed.

3.2.1 Injection fluid and injection pressure

All experiments were performed using vacuum pressure and an industrial circulating oil (*Engen Gencirc 150*). Performing a particular experimental set on the same day ensured a minimal variation in infusion pressure. The oil temperature and therefore viscosity also remained consistent.

A barometer was used to measure daily atmospheric pressure while the temperature and viscosity of the oil were measured using a thermocouple and viscometer (Brookfield - LV series) respectively.

3.2.2 Fabric preforms

For each specific experiment set the RTM and VI setups had the same preform composition. The preform consisted of the same fabric and number of layers. Identical staking sequences, with respect to the orientation of the warp and weft directions, were applied to both the VI and RTM preforms. To ensure experimental consistency the widths of the inlet and outlet configurations were identical for all experiments. Details of the specific preforms are presented in section 3.3.

3.2.3 Dry compacted thickness (VI) and cavity height (RTM)

In the VI process, the thickness immediately ahead at the flow front remains constant as a steady compaction pressure is applied to the dry fabric preform [10]. This consistent thickness is a key component in the present experimental work. For comparative purposes, the cavity height established in the RTM experiment was set equal to the dry compacted thickness measured from the VI experiment which was performed first. The comparable thickness and cavity height is illustrated as “h” in Figure.3.1.

To measure the thickness of a compacted preform prior to the VI experiment, a thickness measurement method was developed. The method uses the difference between two depth measurements to determine the dry compacted thickness. Figure 3.8 shows the measurement method and the measurement components.

Prior to the thickness measurement, two compaction pressure cycles were applied to the fabric preform. This forced the fibres to nest thus establishing a consistent thickness. A depth gauge mounted to a beam spanning transversely across the lower mould was used to measure the compacted preform thickness. The first measurement was taken off to the side of the compressed fabric (zero measurement). The second was measured over the top of the compressed fabric. This method of measurement is possible as the lower mould surface was machined and surface ground flat thus providing an accurate and consistent reference point. However, to increase accuracy, two additional steps were used. Firstly, a glass slide was placed under the measuring spindle. This distributed any force from the spindle over a larger area, avoiding local deformation of the preform. Secondly, the measurement steps were repeated numerous times at various locations. The recorded thickness was then the average of all measurements taken.

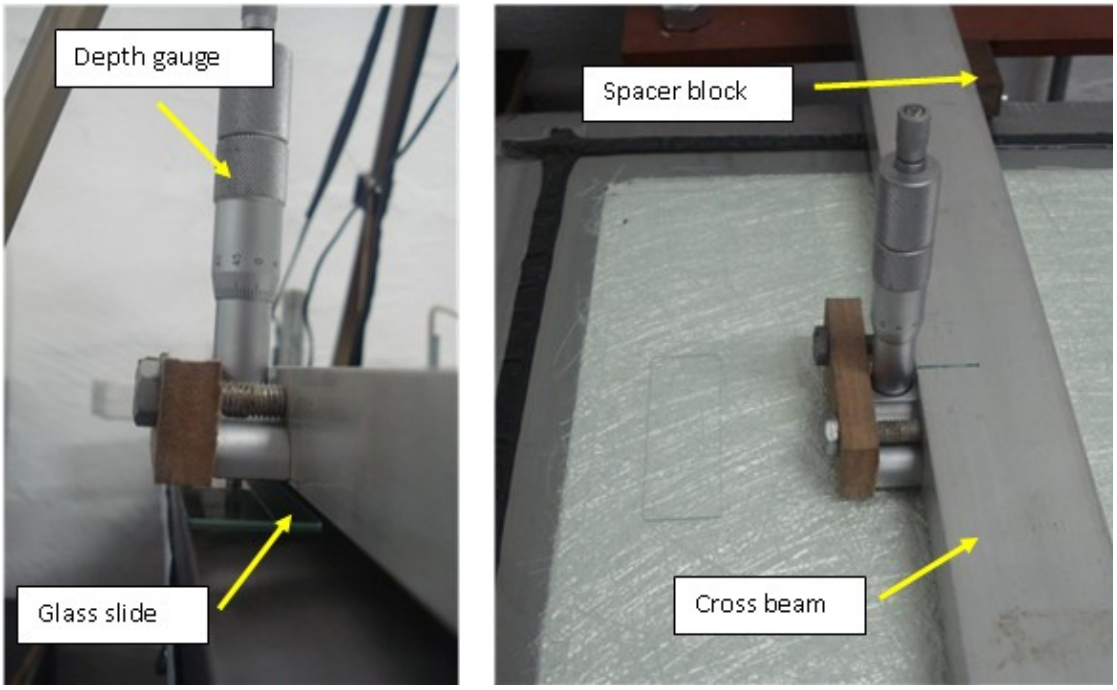

Figure 3. 8 - Measurement of the dry compacted preform thickness (VI)

After the VI experiment was completed, the RTM setup was then configured. The mould cavity was formed between the lower mould surface and a 19 mm thick glass plate. The cavity thickness was set by utilising shim stock (thin metal strips), of various thicknesses, which were stacked together to create the required spacing. The thickness of the individual strips was important in matching the dry compacted thickness accurately when stacked. All shim stock of the same thickness was cut from the same rolled plate. This ensures thickness consistency. To accurately measure the thickness of an individual strip all of the same thickness strips were stacked and measured together. This measurement was then divided by the number of strips in the particular stack to determine the individual strip thickness. The result was a more accurate thickness measurement of an individual strip. Combinations of different thickness shim stock were then used to, as accurately as possible, obtain the measured dry compacted thickness (h) from the VI experiment. The thickness of a preform was used in determining the fibre volume fraction and therefore, porosity using (Eq. 2.21) and (Eq. 2.22).

3.2.4 Displacement and fluid pressure measurement

For the VI experiments, surface displacements and fluid pressures were measured concurrently at four locations during the experiments. Both pressure and surface displacement data are required to characterise the saturated material response behaviour for the various preforms tested. In the experimentation, saturated material response behaviour was observed as surface displacement changes as the fluid pressure increased.

The fluid pressure and displacement measurements were recorded from four measurement couples positioned 30, 50, 100 and 140 mm from the injection channel. The dashed blue lines in Figure 3.1 indicate the positions of the measurement couples.

A measurement couple, shown in Figure 3.9, consisted of one linear variable displacement transducer (LVDT) and a pressure transmitter positioned directly opposite each other. The LVDT applies minimal contact pressure to the vacuum bag as the measurement armature is free floating. The instrument was supported in a specifically manufactured mounting and was suspended from a support frame above the lower mould surface. The pressure transmitter used in the measurement couple was a 4-20 mA loop powered device, manufactured by Wika instruments with a range of 0-2 bar (A). Figure 3.9 shows the transmitter mounted in a tapped hole on the underside of the lower mould surface. The hole for the root diameter of the threads was extended to 5 mm below the top surface. The result is the formation of an oil pocket above the transmitter. Three 1.5 mm diameter holes, positioned directly opposite the transmitter and drilled from the top surface of the tool, allowed oil to pass from the top surface into the oil pocket. The pressure, was thus transferred to the transmitter. The small holes prevented material/fabric from being pressed into the oil pocket and effecting the resulting displacement measurements. The oil pockets were filled with the same oil as the one used in the experiments. The oil pockets were degassed preventing oil from being removed when vacuum was applied to the dry preform before an infusion began. The filled pockets allowed for an immediate pressure response when the fluid reached a measurement position.

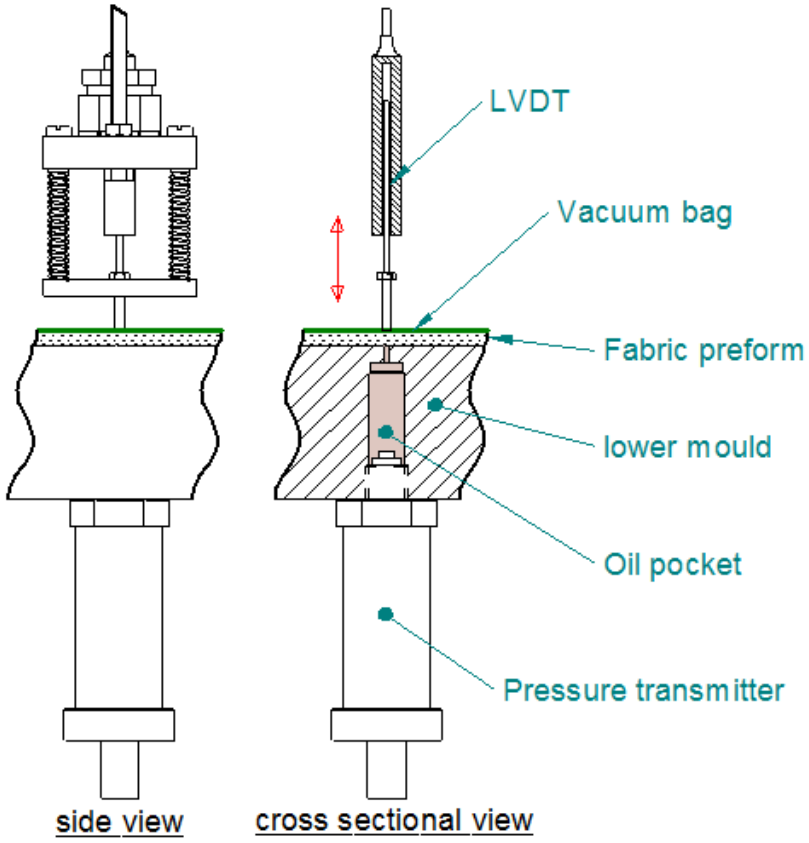

Figure 3. 9 - Measurement couple – LVDT and pressure transmitter

All pressure transmitters and LVDT's were connected to a *National Instruments*, SCXI based, data acquisition system. Device measurements were displayed and recorded using *NI Labview* software. A measurement from each instrument was recorded once per second. By post processing the data, the relationship between bag displacement and fluid pressure could be determined for each of the measurement couples.

Prior to the VI experiment, the LVDT's were positioned directly above the dry compacted fabric preform and opposite the pressure transmitters. The LVDTs output position measurements were set to zero, creating a datum position. All displacement, both positive or negative, were measured from this position. Data logging, from all instruments, commenced when the inlet value opened and the VI experiment began. The LVDT's making up the measurement couples are shown in Figure 3.10.

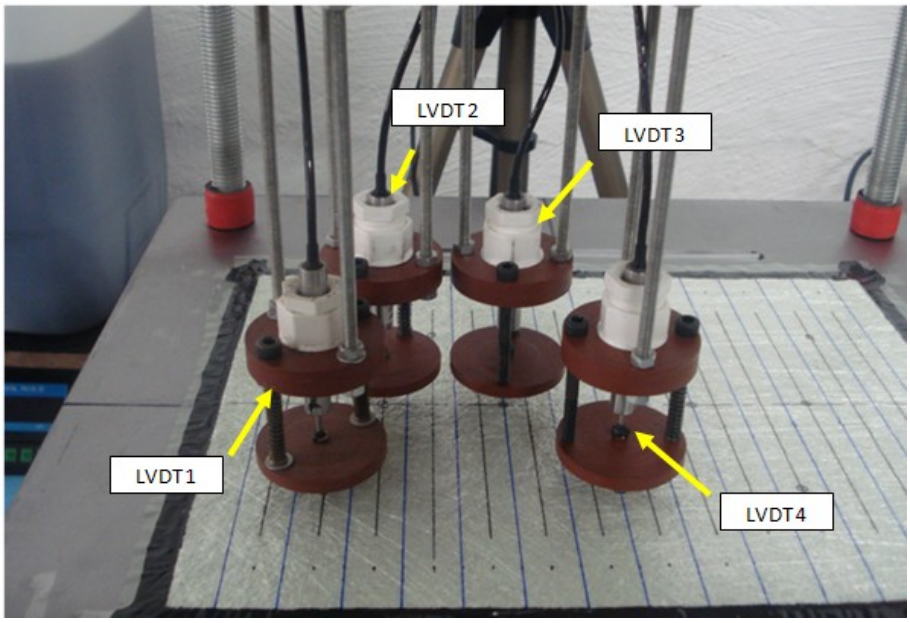

Figure 3. 10 - The LVDT's of the four measurement couples before infusion

3.2.5 Fill time measurement

A reference grid was used to record flow front distances between the inlet to the outlet channel. Based on video captured during the experiment, the changing flow front position was recorded with respect to time to determine flow front propagation.

For the RTM experiments, a transparent film with a reference grid was placed on top of the glass mould surface. However, as surface displacement was measured during the VI experiments, the measurement grid was drawn directly onto the surface of the vacuum bag. The reference grids of the two processes are shown in Figure 3.3.

3.2.6 Fluid mass-time measurement

During VI and RTM experiments, fluid flows into the mould cavity. Measurement of the mass uptake during and after mould filling allows for the mass of fluid present in the mould and flow rates to be calculated. The experiments for which mass uptake was measured are indicated in the experimental section of this work. The mass of fluid entering the mould cavity was measured in terms of the mass change of the fluid leaving a feed reservoir.

A glass beaker was filled with oil and placed on a mass scale (Avery Berkel scale: range 1.5 Kg, accuracy 0.1g) prior to an experiment. Video recording of the experiment allowed for the measurement of the mass remaining in the reservoir and the flow front position to be recorded concurrently with time. To accurately measure the mass present in the mould for a given filled length, it was necessary to subtract the mass and time taken to fill the inlet pipe and inlet channel. This mass and time were determined through review of the recorded video.

3.3 Experiments

The experimental work was categorised into two groups. Each group consisted of experiment sets in which multiple preforms were tested in VI and RTM configurations. The following is a description of the composition of the preforms. The description includes the type of fabric, number of layers and the surface density.

3.3.1 Group 1 – Multiple preforms

For experimental diversity four different types of glass fabric were implimented in Group 1.These four fabrics were, chopped strand mat, twill weave fabric, quadri- axial non-crimp fabric and woven roving fabric. The fabrics and are shown in Figure 3.11.

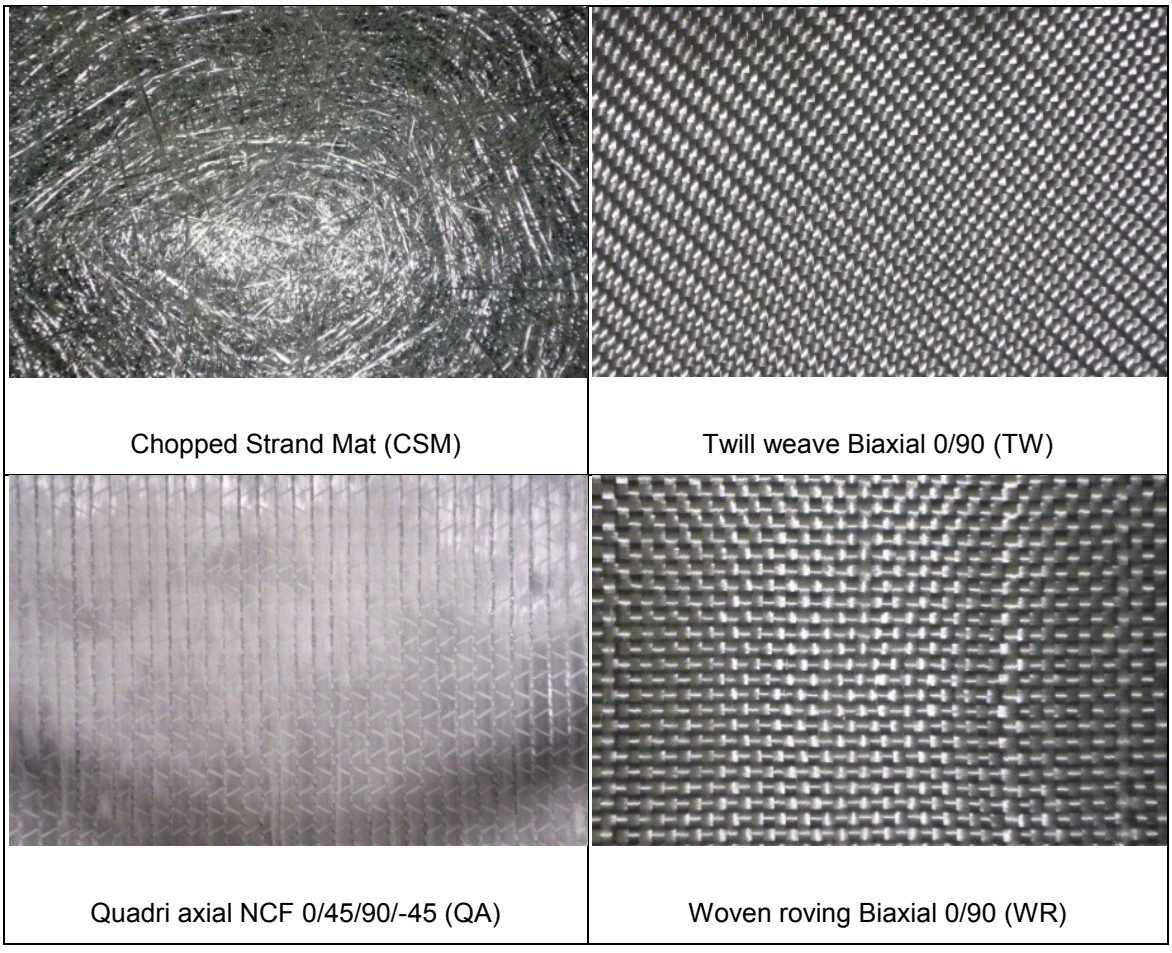

Figure 3. 11 - Fibre glass fabrics

A total of six experiment sets were performed in group 1. Each set consisting of one RTM and one VI test. Table 3.1 displays details specific to each experiment set. The details include the experiment set reference (eg. CSM) followed by composition of the preform which includes; the type of fabric, number of layers (n) and areal density (S_d),

Two values of surface/areal density are shown for each of the fabrics. The first value (S_d*) is that reported by the manufacturer. However, as the magnitude of the areal density is significant in the calculation of fibre volume fraction the surface density was measured from the area of the cut fabric (S_d).

The woven roving fabric was utilised in three experiment sets. The fabric was initially used in five and ten layer layup configurations (WR5 and WR10). The five layer setup was later repeated (WR5-FRM) to investigate the repeatability of material response behaviour and to measure the fluid mass uptake with respect to time.

Exp. Set	Fabric	n	S_d* (g/m^2)	S_d (g/m^2)
CSM	Chopped Strand Mat	8	300	294
TW	Twill weave Biaxial 0/90	4	280	282
QA	Quadri axial NCF 0/45/90/-45	4	1130	1156
WR5	Woven roving Biaxial 0/90	5	450	461
WR10	Woven roving Biaxial 0/90	10	450	461
WR5-FRM	Woven roving Biaxial 0/90	5	450	461

Table 3.1. Group 1 experiment sets.

3.3.2 Group 1 – Single preform

All experiments in Group 2 were performed using the same fabric (woven roving 440 g/m^2 glass fabric) and number of layers (five).

The group consisted of three experiment sets, identified as A, B and C. Each set was conducted on the same day in the same manner as Group 1 experiments. The mass of fluid entering the mould and flow front positions were recorded for all tests performed. Experiment sets A and B each consisted of an RTM and VI experiment. No changes were made to any part of the experimental setups in either process between sets. Therefore, set B is a repetition of experiment set A, performed on a separate day.

Experiment set C consisted of two identical RTM experiments, with only one difference in inlet configuration. The first experiment, like all previous experiments, had fabric overlapping or covering the inlet channel. In the second experiment, the laminate fabric was cut to the edge of the inlet channel. This resulted is no fabric covering the inlet channel.

4. Experimental results

4.1 Group 1 – Multiple preforms

Six experimental sets were performed in Group 1, each set consisted of one VI followed by an RTM experiment. Details regarding the fabric preforms are presented in section 3.3.1. Each set was tested on the same day and under equivalent infusion conditions.

Table 4.1 displays details specific to any particular experiment set. The details include the layup compositions and measured experimental values under which the tests were conducted. The layup composition includes; the type of fabric, number of layers (n) and areal density (S_d), while the experimental measurments include; daily atmospheric pressure (P_{atm}), oil viscosity (μ) and temperature (T), dry compacted thickness (h_{vi}) and cavity height (h_{rtm}).

(Eq. 2.21) was used for the calculation of the fibre volume fractions, where the density of glass was taken as 2547 Kg/m^3. The volume fractions were calculated for both the VI (Vf_{vi}) and RTM (Vf_{rtm}) setups. In the VI configuration the dry compacted thickness (h_{vi}) was used while for the RTM setup the cavity height (h_{rtm}) was used. The measured value of surface/areal density (S_d) was used in the volume fraction calculations.

Exp. Set	n	S_d (g/m^2)	P_{atm} (Pa)	T (^0C)	μ (cP)	h_{vi} (mm)	h_{rtm} (mm)	Vf_{vi}	Vf_{rtm}
CSM	8	294	100652	25	300	2.85	2.858	0.324	0.323
TW	4	282	100312	25	300	0.873	0.872	0.507	0.508
QA	4	1156	100365	25	300	3.425	3.451	0.53	0.526
WR5	5	461	100677	26	273	1.746	1.761	0.518	0.514
WR10	10	461	100598	26	273	3.291	3.31	0.55	0.547
WR5-FRM	5	461	100452	26	273	1.738	1.761	0.521	0.514

Table 4.1 – Group 1 experiment sets

4.1.1 Saturated material response behaviour

Figure 4.1 illustrates the pressure and displacement data obtained from the measurement couples during the VI experiment of the WR5 experiment set. The data is recorded with time and is typical of displacement and pressure behaviour for all of the VI experiments. Post processing the data using the common time referential, it is possible to plot fluid pressure and displacement response for each of the measurement couples. The measurement couple responses are shown for two stages of the infusion.

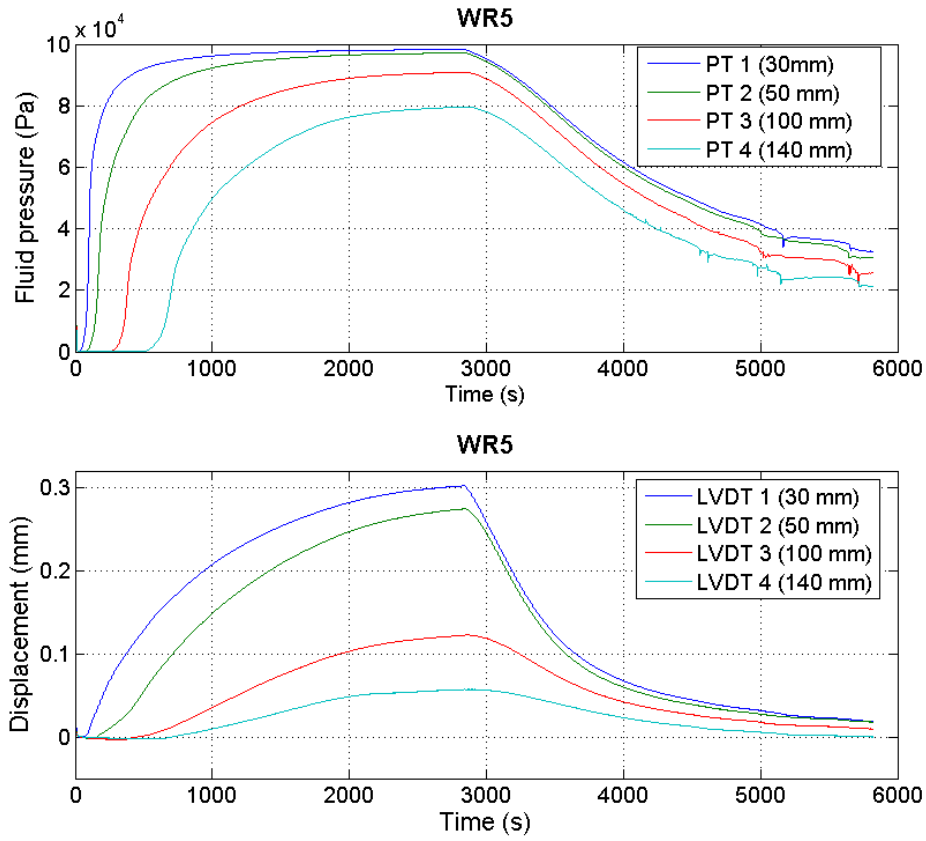

Figure 4. 1 - Pressure and surface displacement data recorded during a VI experiment

In the first stage, inlet and outlet valves were fully open during mould filling. Figure 4.2 illustrates the four measurement couples responses during this period. At the start of the infusion the inlet valve was opened. Air trapped between the feed reservoir and the inlet channel was rapidly drawn into and through the dry preform. The few initial data points in Figure 4.2 are the result of the brief rise in pressures and surface displacements. No

fluid was present at any of the measurement couples. This initial behaviour only lasted for a few seconds and the preform rapidly returned to the original and initial dry compacted thickness. From this compacted position surface displacement and pressure increases as the fluid reached each of the measurement couples. The rise of the fluid pressure consequently resulted in an increase in the thickness of the preform. No saturated nesting of the laminate fabric was recorded during filling, indicating that the dry fabric preform was initially well compacted. The expansion data from all four measurement couples show a consistent relationship between fluid pressure and displacement.

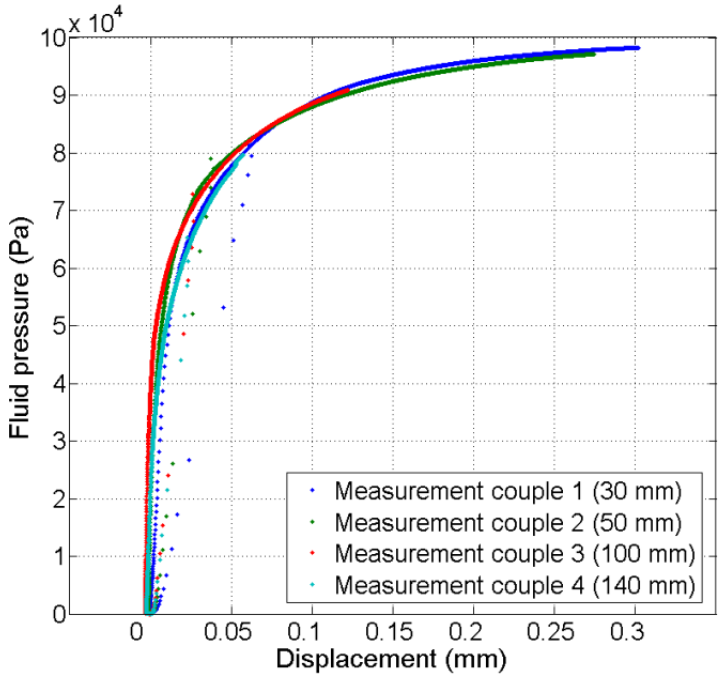

Figure 4. 2 - Measurement couple responses before inlet closure - Saturated expansion

In the second stage of the infusion the inlet valve of the completely filled mould was closed while the outlet valve remained open. Figure 4.3 illustrates the measurement couples responses during this period. The measurement couples show a decrease in fluid pressure and surface displacement, representative of the saturated re-compaction behaviour of the laminate. Unlike the saturated expansion behaviour, the measurement couples measure different displacements for the same fluid pressure. This would indicate that saturated re-compaction behaviour is affected by the saturated expansion history.

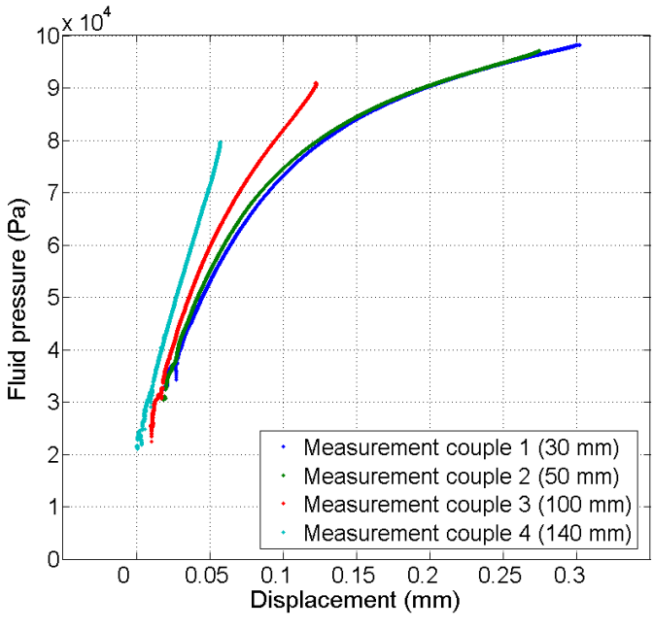

Figure 4. 3 - Measurement couple responses after inlet closure: Saturated re-compaction

The behaviour explained by the saturated expansion and re-compaction of the fabric reinforcement is typical of the response of all the fabrics tested.

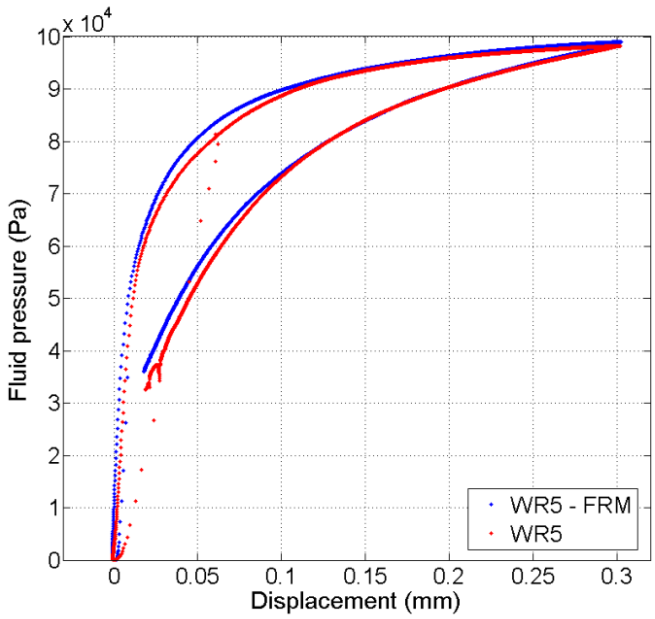

Figure 4. 4 – Measurement couple 1: Data from WR5 and WR5 – FRM experiments

Figure 4.4, shows the pressure displacement measurements of the first measurement couple taken from two VI experiments on the same fabric. The saturated expansion and re-compaction behaviour of the laminate appears to be repeatable. Consequently, for an initially, well compacted and fully nested fabric laminate, it may be possible to determine the relationship between compaction pressure and fibre volume fraction using fluid pressure and laminate thickness data, measured directly from a VI experiment.

The saturated expansion behaviour (Figure 4.2) is used to characterise the material behaviour in the saturated expansion stage which corresponds to the fill stage of the mould cavity. The material characterisation procedure is further described in section 5.1

4.1.2 Pressure distribution behind the flow front

Figure 4.5 illustrates the difference in pressure distribution behind the flow front of the RTM and VI processes. The pressure measurements are extracted from data recorded from the pressure transmitters positioned along the mould length. The transmitters were positioned at distances of 30, 50, 100 and 140 mm from the inlet channel (Figure 3.1)

The measurements for both the RTM and VI tests are shown for an instantaneous flow front position or filled length of 200 mm. The time taken for the RTM process to reach that distance was 466s while the VI test took 553s.

The pressure profile of the RTM process is linear as expected and conforms to (Eq. 2.17). However, the VI pressure profile is curved. The curved profile is a common feature for all VI tests performed. Both RTM and VI pressure profiles are observed to be scalable between the inlet and flow front as the flow front propagates during filling.

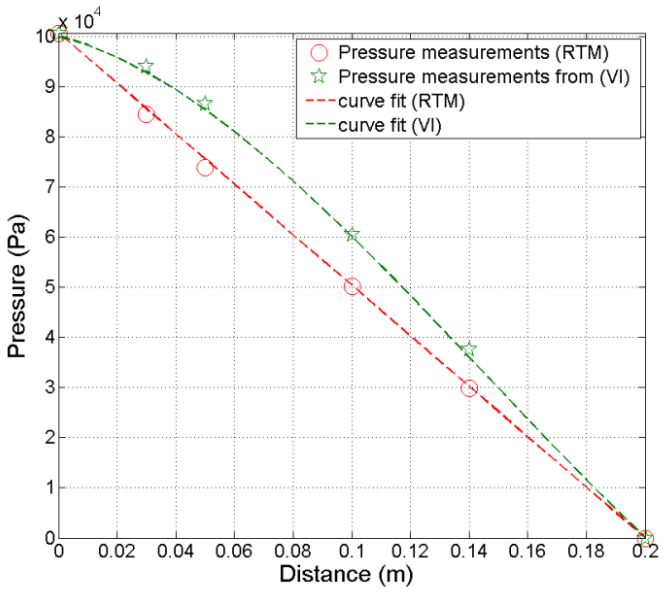

Figure 4. 5 - Pressure measurements at filled length of 200 mm (experiment set CSM)

4.1.3 Fill time results

Fill time, is identified as the time taken for the flow front to reach a particular distance along the mould length. The flow fronts were clearly defined during the experimentation. Figure 4.6 illustrates fill time measurements obtained for five experimental sets performed in Group 1. The circle and star plot points, represent the experimental results of the RTM and VI setups respectively for each of the 5 experimental sets.

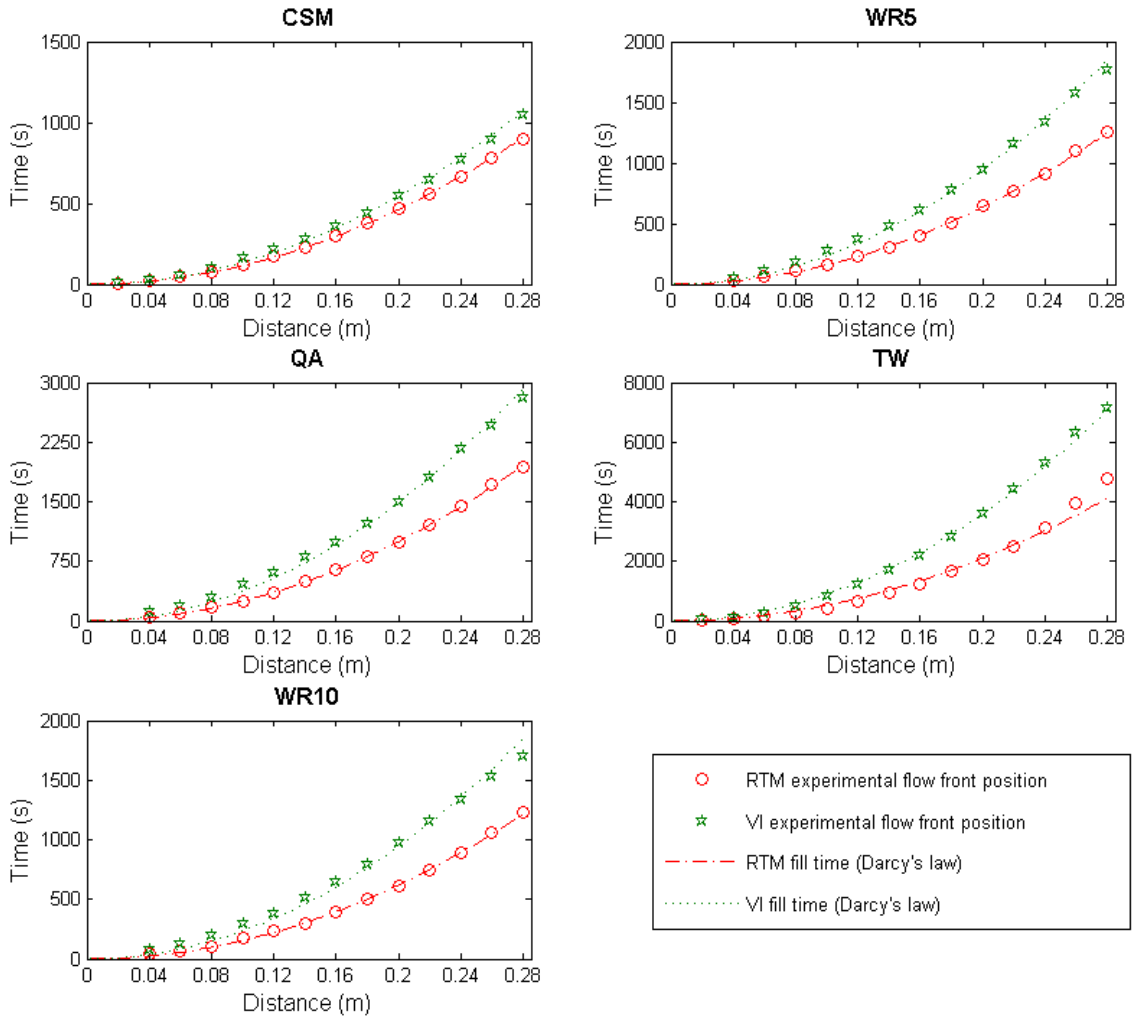

Figure 4. 6 - Fill time results of the experimental sets performed in Group 1

All experiments showed fill time to be proportional to the square of the infusion length. Applying Darcy's law to both the RTM and VI experiments, it is possible to calculate a

permeability for the RTM process and an equivalent permeability for the VI process using (Eq. 2.12). The porosity used in both calculations was that of the RTM case, while the distance-time data was specific to either the VI or RTM experiment. The dotted and dashed lines in Figure 4.6 illustrate the predicted fill times using the calculated permeabilities. It is noted, that for all experiments, flow front progression is slower for the VI process when compared with the RTM process.

To further investigate, the filling behaviour, an experiment set (WR5) was repeated to produce a sixth data set (WR5-FRM). In the repeated experiment, mass uptake with time was measured during both the VI and RTM tests.

In the repeated experimental setup a different inlet feed pipe was implemented. The pipe linked the oil reservoir to the inlet channel. The pipe used for the WR5 experimental set had an internal diameter of 15 mm and a length of 2.1 m. The WR5-FRM experiments utilised a 1m long pipe with an internal diameter of 8 mm.

It was noted that the fill times of the RTM and VI process were affected by the difference in the feed line used. Figure 4.7 illustrates the differences between the fill times for the two VI processes. However, the relationship between fluid pressure and thickness showed repeatability, as shown in Figure 4.4. This would indicate that, the fill times and flow rates, in VI are not only affected by material response behaviour but also inlet feed parameters such as the inlet feed line length and diameter.

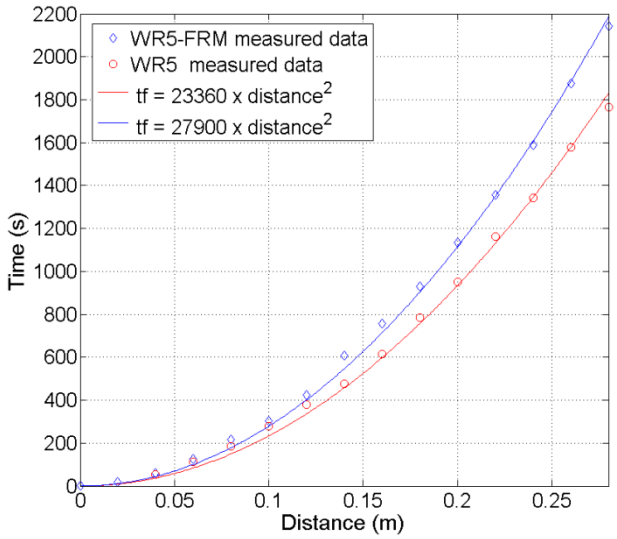

Figure 4. 7 - Fill time results for WR5 and WR5-FRM vacuum infusion experiments

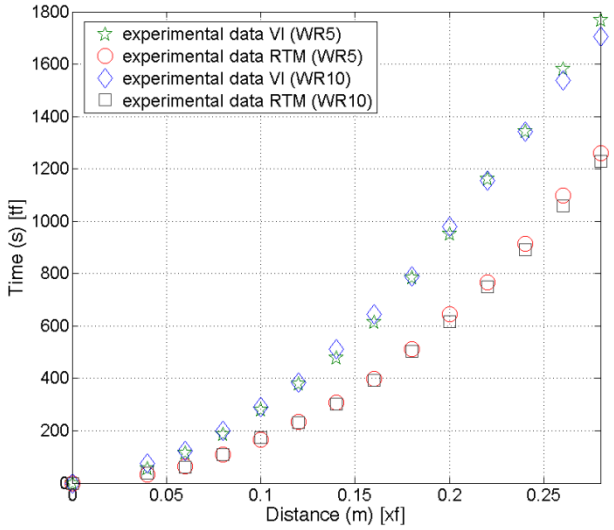

Figure 4. 8 - Comparison of fill times between sets WR5 and WR10

Figure 4.8 illustrates the measured fill times for the RTM and VI tests conducted in the experiment sets WR5 and WR10. The same fabric was used in both preforms with a 5 and 10 layer construction, respectively.

The flow front propagation of the RTM tests (circle and square data points in Figure 5.8) are in line with expected behaviour and conform to Darcy's law. While the thickness of the preform in the two experiments are different the volume fractions/porosity are similar (see table 4.1). As permeability is related to fibre volume fraction/porosity both RTM tests have comparable permeabilities (Eq. 2.37). This results in similar fill times or flow front propagation.

The fill times of both VI experiments (circle and square data points in Figure 4.8) are longer than in the RTM tests. It is noted that the VI experiments demonstrate a similar trend to the RTM results. This highlights that fibre volume and not thickness effect flow in not only the RTM but also the VI process.

4.2 Group 2 - Single preform

4.2.1 Experiment sets A and B

Figure 4.9 illustrates the fluid mass and flow front position variations with time during the RTM and VI experiments performed in experiment set A. The VI experiment exhibited slower flow front progression compared with the RTM case. In both cases, the fill times are proportional to the square of both the fluid mass and infusion length. The relationship is highlighted by the equations for fill times plotted in Figure 4.9. In the figure tf_{vi} and tf_{rtm} are the fill times of the RTM and VI experiments respectively.

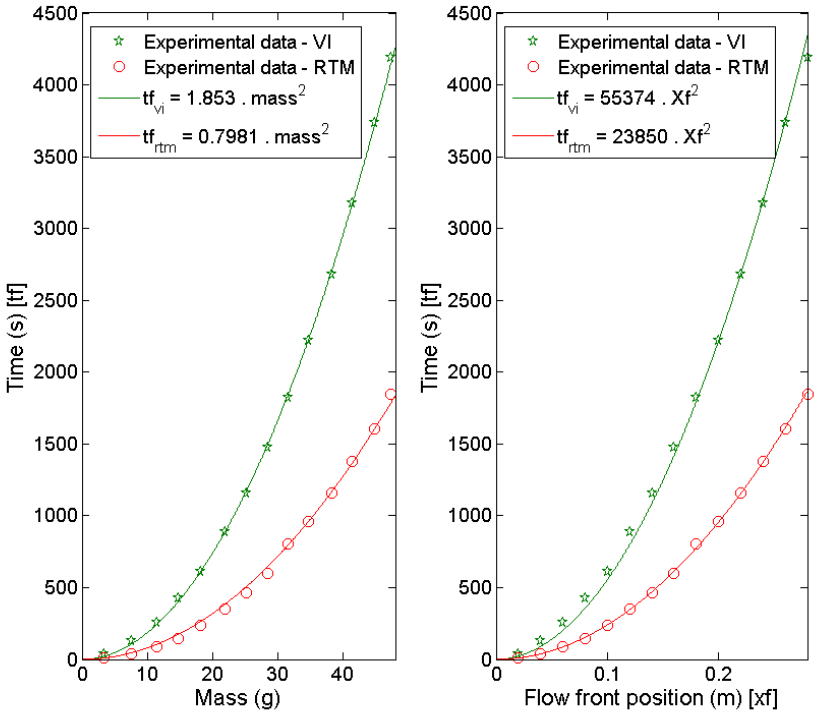

Figure 4. 9 - Experiment set A

The ratio of the fluid mass (g) to filled length (m) remains constant and equates to 173 g/m. This indicates that the same quantity of fluid mass is present for any given filled length in both processes. Therefore, while thickness variation occurs behind the flow front, the increased volume does not result in a significant or measurable mass accumulation during a VI process. It appears that flow front progression is slower in the VI process due to a slower flow rate entering the mould cavity for a given filled length.

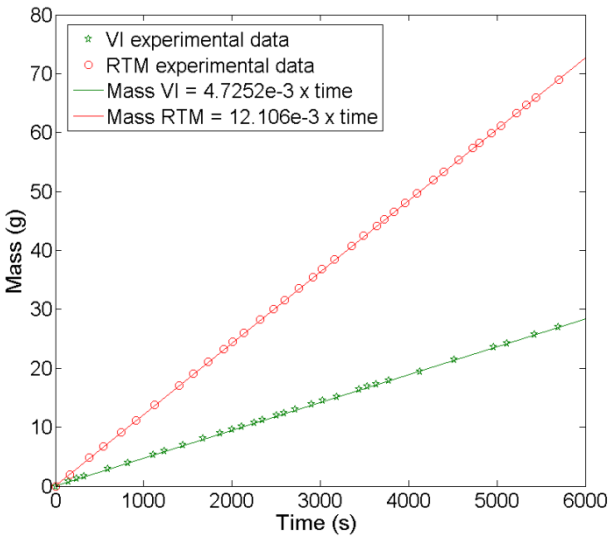

Figure 4. 10 - Experiment set A – Steady state

Figure 4.10 illustrates the steady state mass/time data collected from experiment set A. The mould in both the VI and RTM experiments was completely filled and a steady state flow condition was established. The mass/time relationship is linear, indicating a constant mass flow rate for both experiments. The mass flow rate in the VI setup was again noted to be slower than that of the RTM case even under steady state conditions.

The slower mass flow rate in the case of the VI process which results in slower flow front progression is also present once steady state is established. The implication is that, for thin laminates, VI like RTM could be modelled based on a steady state conditions and Darcy's law.

Figure 4.11 illustrates the mass/time data obtained for identical experiment sets A and B. The plot illustrates the experimental repeatability.

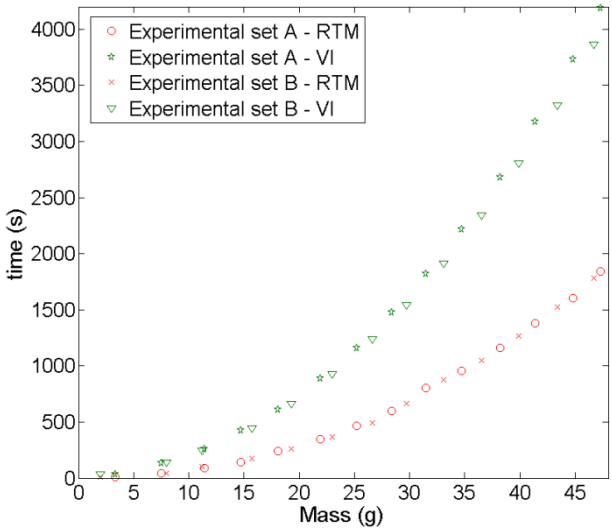

Figure 4. 11 - Experiment sets A and B

4.2.2 Experiment set C

The fluid mass and flow front position of the two RTM experiments of experimental set C, are illustrated in Figure 4.12. As expected, for the RTM process, the fill times are proportional to the square of the infusion length and the mass of fluid present. The covered inlet setup exhibited a slower flow front propagation compared to that of uncovered setup. As the RTM experiments demonstrate the same proportional fill time behaviour, it is possible to model both processes using Darcy's law. However, the values of permeability will be different as the small change to the inlet configuration influences the flow rate when compared with that for the covered experiment.

Figure 4.13, illustrates the steady state mass/time relationship for both the RTM experiments. The differential of the relationship yields the mass flow rates of the two experiments. The covered inlet configuration, exhibits a slower steady state mass flow when compared with the uncovered setup.

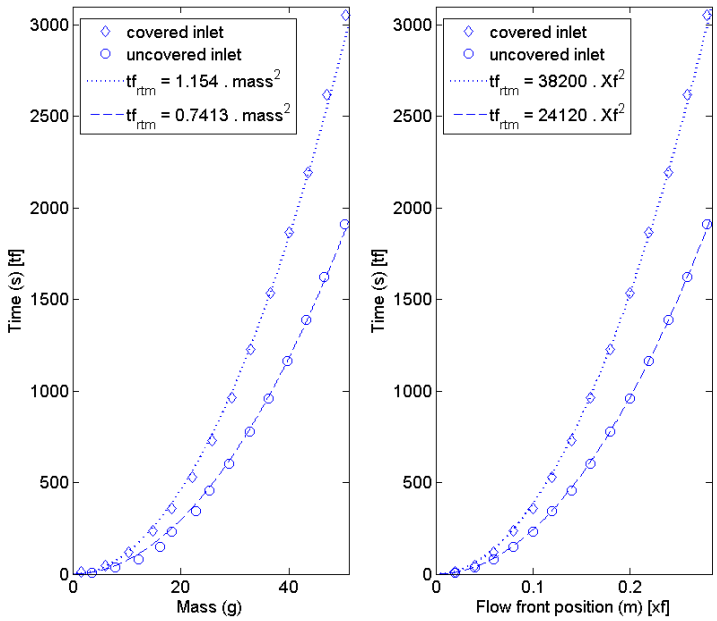

Figure 4. 12 - Experiment set C

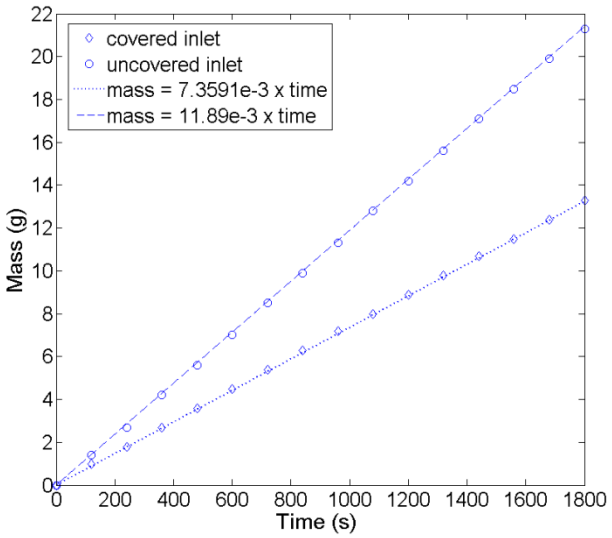

Figure 4. 13 - Experimental set C – Steady state

The experimental set shows that a slight difference in the inlet configuration affects the mass flow rate behaviour in an RTM process. However, Darcy's law can be still be implemented to predict flow front progression and fill times. It is suspected that the flow rate in the VI process could be equally affected if a steady state condition and Darcy's law is implemented to model flow in the VI process.

4.3 Discussion

The experimental work presents a method and experimental setup for the comparison of RTM and VI under equivalent infusion conditions and parameters.

Fluid pressure and thickness variations were recorded during the VI experiments using measurement couples. It was observed that for all fabric preforms tested no saturated nesting occurred during filling. This indicates that the fabrics were fully nested prior to infusion. Therefore, during filling the fabric reinforcement only increased in thickness from its original initial dry compacted thickness with increase in fluid pressure. The saturated behaviour was divided into two stages saturated expansion and saturated re-compaction.

The expansion data from all four measurement couples show a consistent relationship between fluid pressure and displacement (Figure 4.2). In contrast, the saturated re-compaction measurements showed different thicknesses for the same fluid pressure, indicating that re-compaction behaviour is affected by the saturated expansion history (Figure 4.3). However, overall, both saturated expansion and re-compaction response behaviours appear to be repeatable for the same fabric preform under equivalent compaction conditions (Figure 4.4).

Using the saturated expansion data, material response behaviour can be determined through material characterisation. The behaviour is the relationship between the preform thickness/fibre volume fraction and compaction pressure. Material characterisation is discussed in section 5.1 and is required for the evaluation of the VI models presented later.

The pressure distribution/profile is the fluid pressure between the inlet and flow front and occurs during the flow in both RTM and VI. The RTM experiments exhibited a linear pressure profile as expected (Eq.2.17), while a curved pressure profile was observed for the VI experiments (Figure 4.5). The curved profile is attributed to the pressure balancing between the fluid and the fabric preform (Figure 2.4).

For all comparative experiments, slower flow front progression and longer fill times are observed in the VI process (Figure 4.6). The fill times in both VI and RTM are observed

to be, not only, proportional to the square of the infusion length but also to the mass of fluid present in the mould cavity (Figure 4.9).

The mass of fluid to filled length ratio for an RTM process is the same as that of the VI process. This means that for a given mass, the instantaneous flow front positions or filled lengths of both processes are equal. In addition, under steady state conditions (constant filled length) the mass flow rate entering the mould cavity in the VI process is less than in the RTM case (Figure 4.10).

It is hypothesised that while thickness variations occur behind the flow front in the VI process as a result of pressure balancing between the fluid and fabric, it may not be associated with fluid accumulation. Therefore, VI like RTM, could be modelled as steady state flow using Darcy's law, where thickness and permeability are functions of pressure. However, this may only be applicable to thin laminates such as the ones implemented in this study. Thicker laminates, with large thickness variations, may require accumulation effects to be considered in modelling fluid flow.

The flow rates and resulting fill times in the VI and RTM processes are complex and influenced by all aspects of the filled region, from the fluid feed line to the flow front. A repeated experimental set consisting of a RTM and VI experiment, showed that changes to the inlet feed line effected the fill times in both processes (Figure 4.7). While the fill times were different in the VI experiments the saturated material response behaviour was shown to be repeatable (Figure 4.4).

The two identical RTM experiments demonstrated that dynamic and steady state flow rates in the RTM process are affected by minor changes to the inlet configuration (Figures 4.12 and 4.13). The difference in flow behaviour would result in two different permeabilities being determined for the same fabric preform with identical thickness. This demonstrates the susceptibility of permeability measurements to aspects other than the porosity of the fabric. Therefore, the way in which permeability is measured and Darcy's law implemented to model RTM should be given careful consideration.

5. Preform characterisation

Three preforms from three experiment sets were selected from the experimental work to investigate the VI models. For each of the three preforms saturated expansion and permeability behaviour are characterised and modelled. The 3 preforms selected were taken from Group 1 and formed the experiment sets CSM, WR5 and QA.

5.1 Material characterisation – saturated expansion

The relationship between laminate thickness/fibre volume fraction and compaction pressure is complex and is affected by numerous factors. The following outlines the method used to extract thickness and compaction pressure data directly from the VI experiments performed in an experiment set. The extracted data is then fitted to the power law model proposed by Robitaille et al [52]. As the models investigated in this work deal with the filling stage of the VI process, only the saturated expansion behaviour is characterised and modelled.

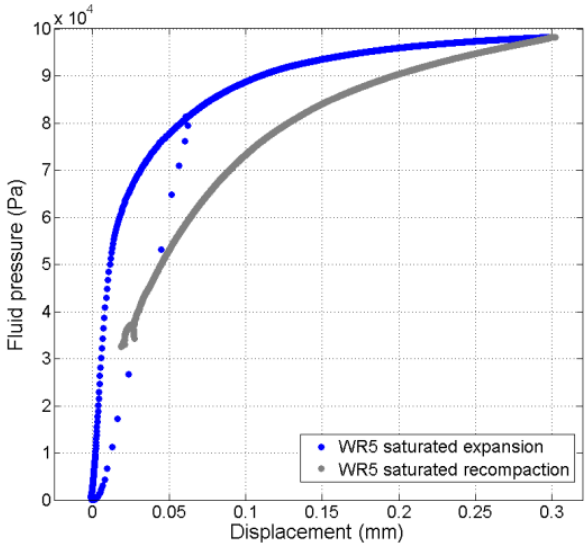

Figure 5. 1 - Measurement couple 1 – experimental data for WR5 experiment

Figure 5.1 illustrates the fluid pressure and surface displacement measured from a measurement couple during the filling stage of a VI experiment. It is observed that thickness only increased from the initial dry compacted position (zero position) as fluid pressure increased. Stated differently, no saturated nesting occurred during the fill stage. This indicates that the initial dry compaction stage fully nested and compacted the preform fabric.

Through manipulation of the surface displacement and fluid pressure measurements (Figure 5.1) it is possible to convert the displacements to thickness/fibre volume fraction data and fluid pressure measurements to compaction pressure data.

To convert the surface displacement measurements to thicknesses the initial dry compacted and measured laminate thickness (h_f) is added to all displacement measurements (δ) (Eq. 5.1). The resulting thickness (h) measurements convert to the corresponding fibre volume fractions using (Eq. 2.21).

$$h = h_f + \delta \tag{5.1}$$

To convert the fluid pressure (P) measurements to compaction pressure (P_{comp}) data the Terzaghi equation (Eq. 2.20) is utilised. The atmospheric pressure (P_{atm}) on the day of each of the VI experiment is used in the calculation.

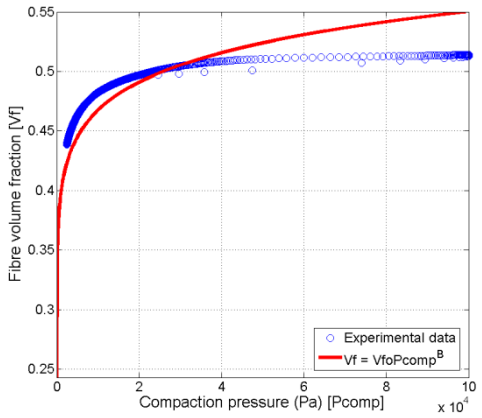

Figure 5. 2 - Compression response behaviour for WR5 – saturated expansion

The new experimental data derived through the conversion process is illustrated by blue marks in Figure 5.2 for the WR5 fabric preform. This data is fitted to the power law model (Eq. 2.36) using a Matlab curve fitting utility [55]. The utility implements a nonlinear least squares method to determine the values of V_{f0} and B in a parametric fit with Eq. 2.36. Figures 5.3 and 5.4, illustrate the results from the other two fabric preforms selected for the present work. V_{f0} is the fibre volume fraction at a compaction pressure of 1Pa. B is the exponent and referred to as the stiffening index of the fabric. Table 5.2 displays the values of V_{f0} and B determined for all 3 preforms.

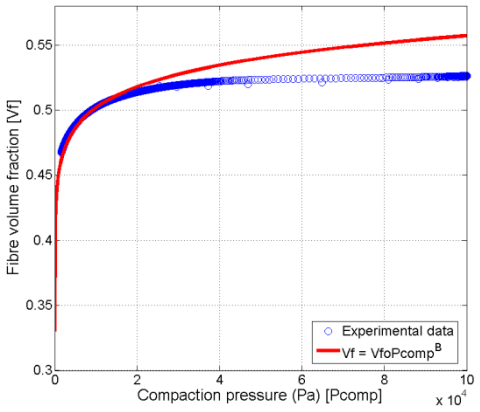

Figure 5. 3 - Compression response behaviour for QA – saturated expansion

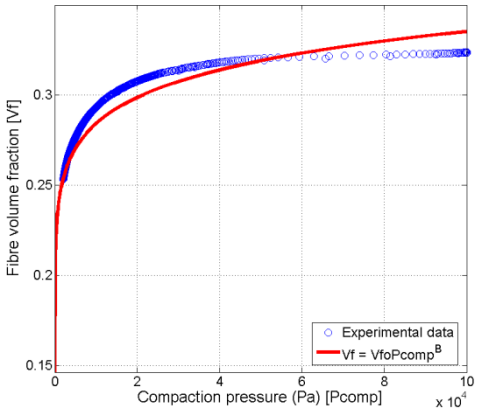

Figure 5. 4 - Compression response behaviour for CSM – saturated expansion

Material characterisation model inputs (saturated expansion)

Exp. Set	Fabric	V_{fo}	B
CSM	Chopped Strand Mat	0.1464	0.072
QA	Quad axial NCF 0/45/90/-45	0.33	0.04548
WR5	Woven roving Biaxial 0/90	0.243	0.071

Table 5.1 – Material characterisation of three fabric preforms

5.2 Permeability characterisation

Thickness and fibre volume fraction change during the VI process resulting in permeability variations. It is therefore necessary to characterise and model this behaviour. Eq. 2.37 is widely used to characterise the relationship between permeability and fibre volume fraction. To model the behaviour for a given fabric preform, it is necessary to calculate the value of the Kozeny constant (k_0).

Each of the three experiment sets consisted of one VI and one RTM process. Both processes in each set implemented exactly the same preform composition. The consistent cavity height of the RTM process allows for the fibre volume fraction and porosity of the preform to be determined. Then from Eq. 2.12 the preform permeability is calculated using experimental fill time data.

This permeability value and corresponding fibre volume fraction are used to determine the Kozeny constant from Eq. 2.37. Table 5.2 illustrates the permeabilities, fibre volume fractions and Kozeny Carmen constants derived for the three fabric preforms under investigation.

Exp. Set	Fabric	Permeability	Fibre volume fraction	Porosity	Kozeny constant
		K	V_f	ϕ	k_0
CSM	Chopped Strand Mat	8.7145×10^{-11}	0.324	0.676	2.9618×10^{-11}
QA	Quadri axial NCF 0/45/90/-45	2.8346×10^{-11}	0.526	0.474	7.3809×10^{-11}
WR5	Woven roving Biaxial 0/90	4.1109×10^{-11}	0.514	0.486	9.4578×10^{-11}

Table 5.2 Permeability characterisation of three fabric preforms

Ideally, permeability characterisation should involve multiple permeability experiments performed on the same preform at various thicknesses/porosities. However, for the present work the characterisation method described above is acceptable. The Kozeny constant (k_0) obtained of the non crimp Fabric (NCF) Quadriaxial is 7.3809×10^{-11},this is in line with a reported value of 7.18×10^{-11} for Non crimp fabrics [10].

6. Evaluation of VI models

For all the VI models, the permeability (K) and laminate thickness/cavity height (h) are both functions of pressure (P). The compaction pressure (P_{comp}) is related to fluid pressure through Eq. 2.20.

Eqs. 6.1 and 6.2 illustrate the formulation for h and K in terms of compaction pressure. The differentials of these equations with respect to fluid pressure are shown in Eq. 6.3 and 6.4 respectively.

Substituting Eq. 2.36 into Eq. 2.21 yields

$$h = \frac{n\, S_d}{\rho V_{f0}\, P_{comp}^{B}} \tag{6.1}$$

Substitute Eq. 2.36 into Eq. 2.37 yields

$$K = \frac{k_0 \left(- \left(V_{f0} P_{comp}^{B}\right)^3 + 3\left(V_{f0} P_{comp}^{B} \right)^2 - 3\left(V_{f0} P_{comp}^{B}\right) + 1 \right)}{\left(V_{f0} P_{comp}^{B}\right)^2} \tag{6.2}$$

Differentiating Eq. 6.1 with respect to fluid pressure yields Eq. 6.3

$$\frac{dh}{dP} = \frac{n\, S_d\, B}{\rho V_{f0} \left(P_{comp}\right)^{(B+1)}} \tag{6.3}$$

Differentiating Eq. 6.2 with respect to fluid pressure yields Eq. 6.4

$$\frac{dK}{dP} = k_0 B \frac{\left({V_{f0}}^3 \left(P_{comp}\right)^{B-1} - 3V_{f0} \left(P_{comp}\right)^{-(B+1)} + 2\left(P_{comp}\right)^{-2B-1} \right)}{{V_{f0}}^2} \tag{6.4}$$

6.1 Input data

In order to implement the Equations 6.1-6.4 in the VI models, input data specific to each of the three fabric preforms is required.

The density of the fabric, number of layers and surface/areal density are properties of the composition of each of the preform layups (Table 5.1). The thickness and permeability changes due to compaction pressure are modelled using Eqs. 6.1 and 6.2 respectively. The values of V_{f0}, B and k_0 are derived from experiments through material and permeability characterisation. Tables 5.1 and 5.2 illustrate the specific values of each of the three preforms.

The VI models (Eqs. 2.30, 2.31, 2.35) also required boundary conditions to be specified. The inlet pressure (P_{in}) is specified as the daily atmospheric pressure (P_{atm}) while the pressure at the flow front (P_{out}) is specified as vacuum (0Pa).

6.2 Solution method

All three VI models are differential equations (Eqs. 2.30, 2.31, 2.35) which share the same general form. The equations are second order non linear boundary value problems (BVP). Solution of the models requires the implementation of numerical methods.

Corriea et al [10] solved Eq. 2.30 using a finite difference method. The method replaces the derivatives in the BVP with finite difference approximations. The solution domain is divided into sub-intervals by grid points or nodes. The differential equation is then written at each of the interior nodes in the solution domain. This results in a system of nonlinear algebraic equations. The solution of the system is a numerical solution of the differential equation [55].

Modi [26] solved Eq. 2.31 using the shooting method. The method converts the second order BVP equation into two first order initial value equations. If the initial condition for each of the initial value equations is known, the equations can be solved numerically. For the BVP, boundary conditions are specified at the first point and at the end point of the solution domain. The boundary condition at the first point is used as an initial condition in the solution of the two initial value equations. As two equations are

present, an additional initial condition is required and is initially guessed. The system of initial value equations is solved and the solution obtained at the end point is compared with that specified in the BVP. If the end point solution derived numerically is not accurate enough, the guessed initial condition at the first point in the solution domain is changed and the system is solved again. The process is repeated numerous times until the numerical solution agrees with the boundary condition prescribed at the end point of the domain [55]. The author solved the system of initial value problems using two numerical methods (Euler and fourth order Runge-Kutta) and at two discretisation levels (100 and 1000 nodes) to investigate accuracy and convergence of the solution. The solution was not affected by the numerical method or the discretisation level used.

In the present work, all VI models are solved using a Matlab built-in function named bvp4c. The Matlab function is based on the finite difference method [55, 56]. Solution of a BVP using "bvp4c" requires two additional functions and several solution parameters to be specified. The functions include the BVP itself and a function for calculation of the residual. The residual function calculates the difference between the numerical solution and the prescribed boundary condition. The discretisation level and boundary conditions are also specified.

7. Results of the VI models

The following is a discussion of the solutions of the VI models (Eq. 2.30, 2.31, 2.35). The results are categorised into pressure profile, thickness variations and fill times predictions and are compared with the corresponding VI experiment.

7.1 Pressure profiles

The solution to the VI models yields the pressure profile behind the flow front spanning from inlet to the flow front.

It is noted that for the accumulation based models (Eq. 2.30, 2.31) the glass density (ρ), surface density (S_d), kozeny constant (k_0) and number of fabric layers (n) cancel. As a result these model inputs do not affect the pressure profile solution. However, the values are necessary in the determination of the fill time and flow front progression. The pressure profiles are also scalable from any given filled length [10, 27]. It is observed that the non-accumulation steady sate model (Eq. 2.35) presents the same behaviour as the two accumulation based models.

Figures 7.1–7.3 illustrate the numerical solutions of the three VI models using input data extracted from three VI experiments. The pressure profiles are compared with pressure measurements taken from the corresponding VI experiment. The pressure measurements are recorded at the pressure transmitters located at distances of 30, 50, 100 and 140 mm along the mould length. The pressure data shown in the figures corresponded to flow front positions or filled lengths of 200 and 260 mm respectively. Dividing the pressure measurement locations by the filled length allows from the pressure data to be plotted as the non dimensional positions on the x-axis in the figures.

The curved pressure profile of the VI process is the result of pressure balancing between the fluid and fabric preform. During filling this results in a thickness variation behind the flow front. In contrast, the fixed cavity process (RTM) yields a linear pressure profile in line with equation 2.17 and represented by the dashed lines in Figures 7.1–7.3.

The input data used in all the VI models is identical for each of the three VI experiments. The pressure profile solutions plotted in each figure show that differences

between the models are small. In addition, all the model solutions reasonably agree with the experimental pressures measured in each of the VI experiments.

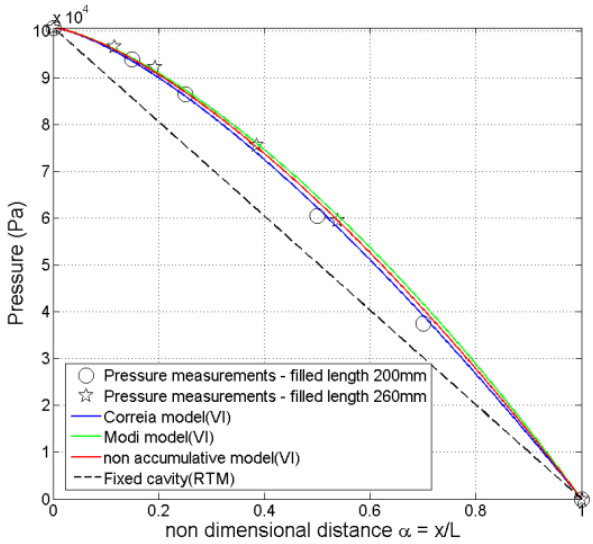

Figure 7. 1 - CSM pressure profile solution

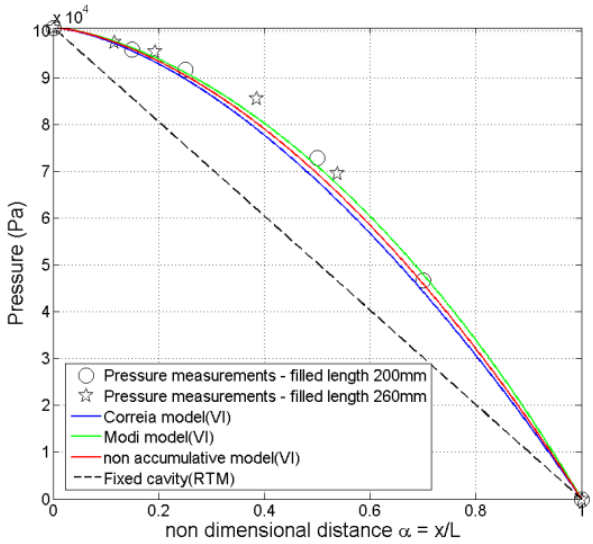

Figure 7. 2 - WR5 pressure profile solution

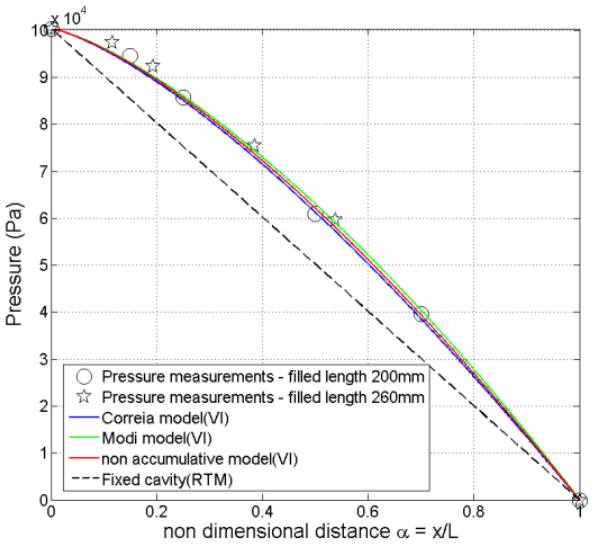

Figure 7. 3 - QA pressure profile solution

7.2 Thickness variations

Figure 7.4 - 7.6, illustrate the thickness variation between the inlet and flow front for the three fabric preforms used to investigate the VI models. The figures represent a filled length of 200mm.

The blue line in each figure is formed from the solution of the steady state non accumulation model (Eq.2.35). The solution of model is the pressure distribution behind the flow front. The pressure profiles of the three fabrics are presented in section 7.1. From the pressure profile solution, a preform thickness profile between the inlet and flow front can be determined using Eq. 6.1 and 2.2. The thickness profiles are shown as blue lines in Figures 7.4 - 7.6. The red points in the figures are thickness measurements taken at the 4 measurement couple locations for an instantaneous flow front position of 200mm. Good agreement is obtained between the solution prediction and the actual measurements.

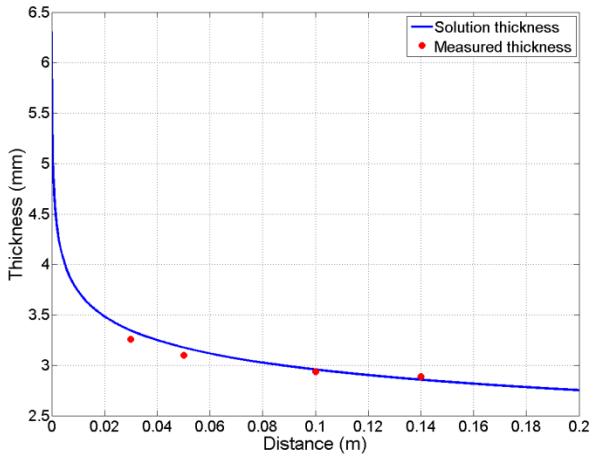

Figure 7. 4 - Comparison of thickness variation with experimental data (CSM)

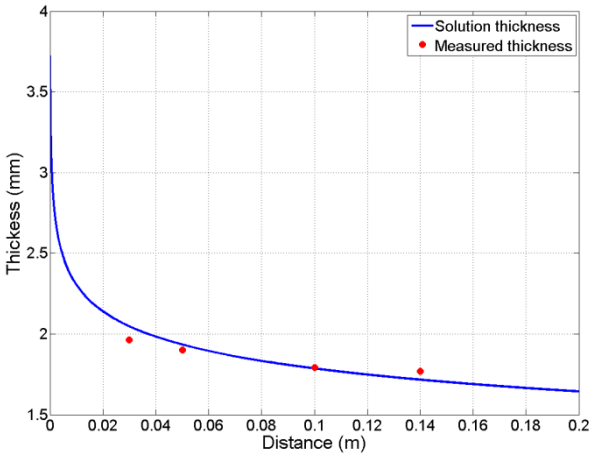

Figure 7. 5 - Comparison of thickness variation with experimental data (WR5)

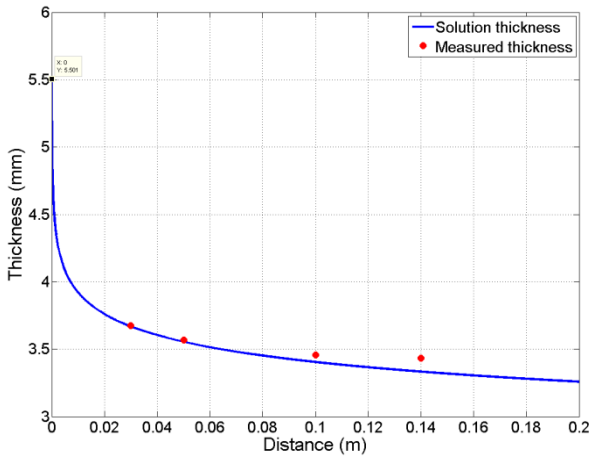

Figure 7. 6 - Comparison of thickness variation with experimental data (QA)

7.3 Fill time behaviour

Correia et al [10] proposed that the pressure gradient at the flow front governs the flow front progression and therefore fill time in the VI process. As shown in Figures 7.1 - 7.3, the pressure gradient at the flow front (α= 1) is larger in VI than in the RTM process. The analytical formulations drew comparisons between the fixed cavity, incompressible RTM, and the VI processes. It was suggested that if the thickness at the flow front in VI were the same as the thickness in a fixed cavity RTM experiment, the permeabilities would be the same (K_{RTM} = $(K_{VI})_{\alpha=1}$). Then due to larger pressure gradient of the VI process the flow front would progress faster than in the RTM case. As the pressure gradients are different but scalable with flow front progression, it is possible to determine a constant of proportionality between fill times and permeabilities of RTM and VI.

The experimentation performed in the current research investigates the above proposal through experimental flow comparison between RTM and VI. The fill times of three experiment sets used to evaluate the VI models are shown in Figures 7.7- 7.9. Each set consisted of one VI and one RTM experiment. In contrast to the proposed filling behaviour, the fill times were longer for the VI experiments. This indicates slower flow front progression in the VI process compared with RTM. This behaviour is observed for all of the experiment sets (Figure 4.6). However, the fill times of the VI process as with RTM are proportional to the square of the infusion length as illustrated in the Figures 7.7- 7.9. It is therefore possible to determine a constant of proportionality between the VI and RTM fill times. It is therefore possible to determine a permeability for the RTM case and an effective permeability for VI if the porosity is assumed constant at the flow front between the two processes (Eq. 2.12).

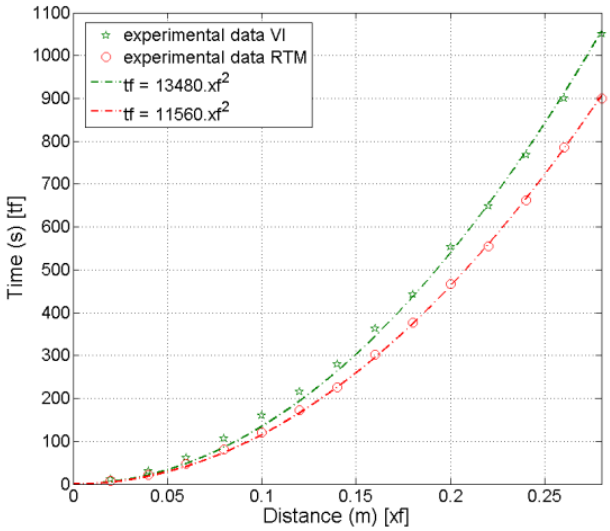

Figure 7. 7 - CSM fill times

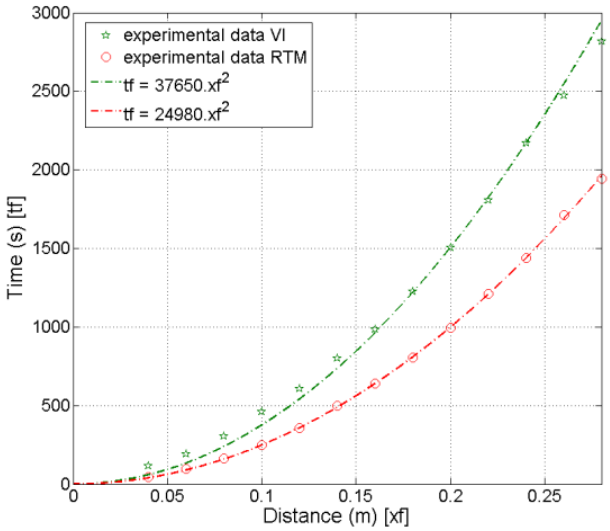

Figure 7. 8 - QA fill times

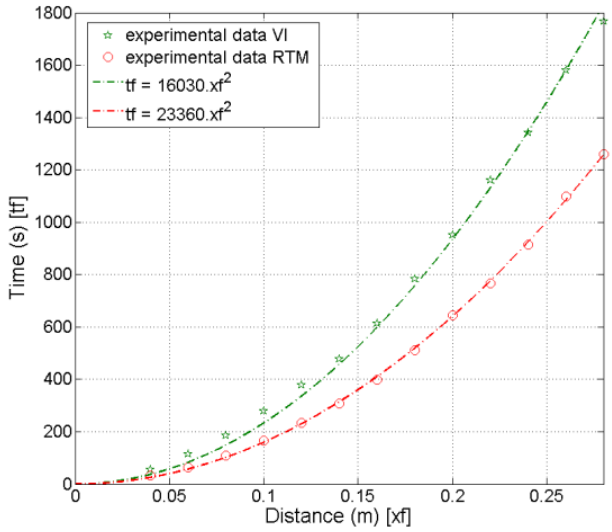

Figure 7. 9 - WR5 fill times

From the experimental work it is shown that no significant fluid accumulation occurs in VI and like the RTM process a constant flow rate is established for a given filled length (Figures 4.9 & 4.10). The flow rates of both processes are also directly proportional to the filled length. During filling, the reduced flow rate in VI manifests as slower flow front progression and longer fill times.

The pressure profile in VI is the direct consequence of pressure balancing between the fluid and fabric and is scalable with filled length. It is shown that a non accumulation based model can be used to predict the pressure profile/distribution behind the flow front. This is a further induction that non accumulative behaviour can be implemented to characterise the VI process.

Considering the filling behaviour of RTM and VI in a direct comparison. Correia et al [10] proposed that the flow front controlled the fill time behaviour and that in a direct comparison between VI and RTM the fill times would be shorter for VI thus implying a faster flow front progression. However, as shown in the experimental work this is not the case. The fill times of VI are shown to be longer than that of the equivalent RTM case. In addition the longer fill times of the VI process are the result of a reduced flow rate entering the mould cavity for a given filled length.

It is proposed that the flow rate in VI is controlled by the inlet and not the flow front as suggested by Correia [10]. The flow behaviour is explained as follows:

The flow rate (q) at the inlet is given by Eq. 7.1 and is the product of the Darcy velocity at the inlet (u_i) and the total inlet/entry or feed area (A_{Ti}).

$$q = u_i \, A_{Ti} \qquad (7.1)$$

Substituting the expression for Darcy's velocity into Eq.7.1 yields

$$q = \frac{K}{\mu} \frac{dP}{dx} A_{Ti} \qquad (7.2)$$

As the inlet channel for both the RTM and the VI experiments were common in the direct flow comparison. The total inlet/entry or feed area (A_{Ti}) remained constant in both processes. The area can then be cancelled from q.7.2. This simplifies Eq.7.2 to Eq.7.3 with only the velocity term remaining. Any variation in the flow rate between RTM and VI must then be the consequence of differences in this inlet velocity.

$$u_i = \frac{K}{\mu} \frac{dP}{dx} \qquad (7.3)$$

Assuming that the viscosity remains constant, the velocity through the inlet/feed or entry area is the product of two quantities, the magnitude of the permeability (K) and the pressure gradient at the inlet (dP/dx).

During flow, the fabric at the inlet is un-compacted (saturated relaxation) due to the increase in fluid pressure. As a result the permeability at the inlet is significantly increased. The increased inlet permeability remains constant during filling. However, concurrently a scalable pressure profile is established between the inlet and the flow front. This pressure profile exhibits a substantially reduced pressure gradient at the inlet. The inlet pressure gradient is also scalable with filled length in the same manner as the pressure profile. The pressure distribution and pressure gradient are solely the result of pressure balancing between fluid and compaction pressures.

Consequently the combination of the increased permeability and reduced pressure gradient at the inlet combine to determine the inlet velocity which in turn results in a flow rate through the constant inlet area. As the pressure gradient is scalable with filled length, the flow rate in VI, like RTM, is directly proportional to the filled length. During

the transient or filling stage the flow rate effect results in the fill times of both processes being proportional to the square of the filled length.

It should be noted that the net effect of both the increased permeability and the reduced pressure gradient is that a slower flow rate is established for VI. The reduced flow rate manifests itself as longer fill times when directly comparing the two processes.

In support of the proposed filling behaviour, two experiment sets CSM, WR5 were considered. Explained here is the method applied in the evaluation of the proposed behaviour. Each set consisted of one RTM and one VI experiment tested under identical flow parameters and conditions on the same fabric preform composition.

A filled length of 200 mm was considered in the evaluation. The filled length is arbitrary as both the pressure profiles and resulting inlet pressure gradients are both scalable between the inlet and flow front position.

Considering the RTM experiments, utilising the fill time results and porosity for a given preform the value of permeability (K_{RTM}) is calculated. The pressure gradients (dP/dx) of the RTM experiments is given as the atmospheric pressure applied at the inlet divided by the filled length of 200mm. The fluid velocity (U_{RTM}) of the RTM experiments is calculated from Eq.7.3 and is the same at any point in the filled region including the inlet. The established values for each of the RTM experiments is shown in Table 7.1.

As the inlet area is the same in both RTM and the VI experiments, change in the flow rate must be equal to the variation in the inlet velocity. As the differences in the flow rate are manifest in the fill time behaviour a fill time factor can be determined relating the inlet velocity of the RTM (U_{RTM}) to that of VI experiments (U_{VI}).

As the fluid pressure at the inlet in VI tends toward zero the inlet permeability is significantly increased. The inlet permeability is calculated from Eq.7.4 by setting the compaction pressure (P_{comp}) equal to 1 Pa. The values of k_0 and V_{f0} for both fabric preforms are discussed in the preform characterisation of section 5. This inlet permeability remains constant during filling. The inlet velocities as well as the calculated increased inlet permeabilities of the VI experiments are shown in Table 7.1.

$$K = \frac{k_0\left(-\left(V_{f0}P^B_{comp}\right)^3 + 3\left(V_{f0}P^B_{comp}\right)^2 - 3\left(V_{f0}P^B_{comp}\right) + 1\right)}{\left(V_{f0}P^B_{comp}\right)^2} \qquad (7.4)$$

The permeability distribution for the CSM vacuum infusion experiment is shown in figure 7.10. The constant inlet permeability is highlighted in the figure and remains constant regardless of the filled length.

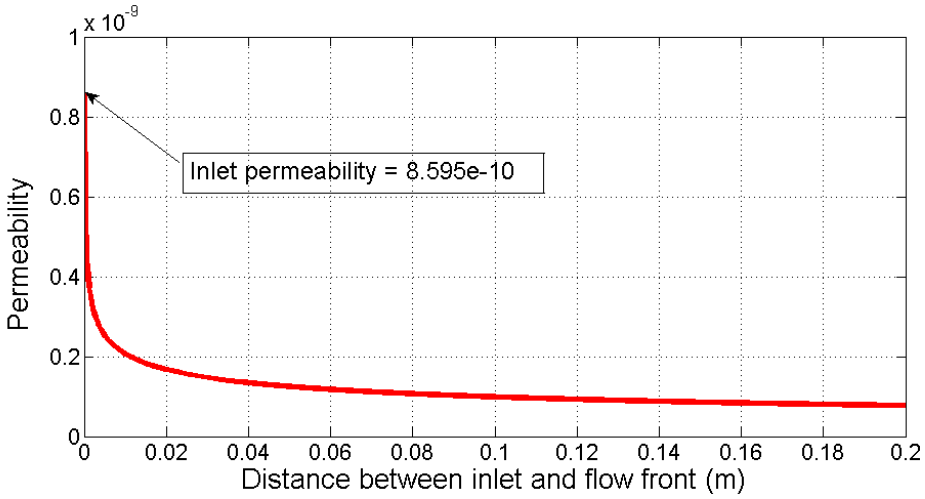

Figure 7. 10 - Permeability distribution of CSM experiment at filled length of 200 mm

From the tabulated values of inlet velocity and increased permeability of the VI tests it is possible to determine the inlet pressure gradients through implementation of Eq. 7.3. The two calculated pressure gradients of the VI experiments are included in Table 7.1.

	Inlet conditions			Fill time factor	Inlet conditions		
	Permeability	Pressure gradient	velocity		velocity	Permeability	Pressure gradient
	K	(-) dP/dx	U_{RTM}		U_{VI}	K	(-) dP/dx
	($x10^{-11}$)	($x10^{3}$)	($x10^{-6}$)		($x10^{-6}$)	($x10^{-10}$)	($x10^{3}$)
CSM	8.715	503.260	146.189	0.858	125.367	8.595	43.758
WR5	4.111	503.390	68.980	0.686	47.334	6.948	20.438
	RTM				VI		

Table: 7.1 – inlet conditions of RTM and VI

The calculated inlet pressure gradients can be compared with the pressure variation at the inlet of the VI experiments. Figures 7.11 and 7.12, illustrate the pressure distribution of the RTM and the VI experiments at the filled distance of 200 mm with the inlet pressure equal to atmospheric. The VI pressure profile is shown in green and is determined from the non accumulation based model while the linear pressure distribution of RTM is shown in red. Two additional dashed lines are also plotted in each of the figures and are a visual representation of the inlet pressure gradient of both processes. The red dashed line is the RTM pressure gradient while the blue dashed line is that of VI. Each figure contains two plots. The data and lines in each plot are identical. The left hand side plot illustrates the data over the complete filled length of 200 mm. The right hand side plot shows an enlargement of the inlet region and the first 5 mm of the filled length.

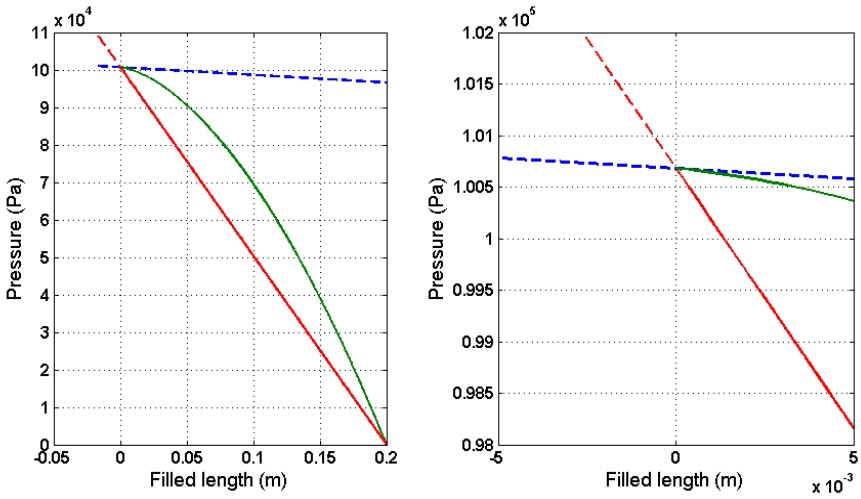

Figure 7. 11 - Pressure profiles and inlet pressure gradients of WR5 experiments

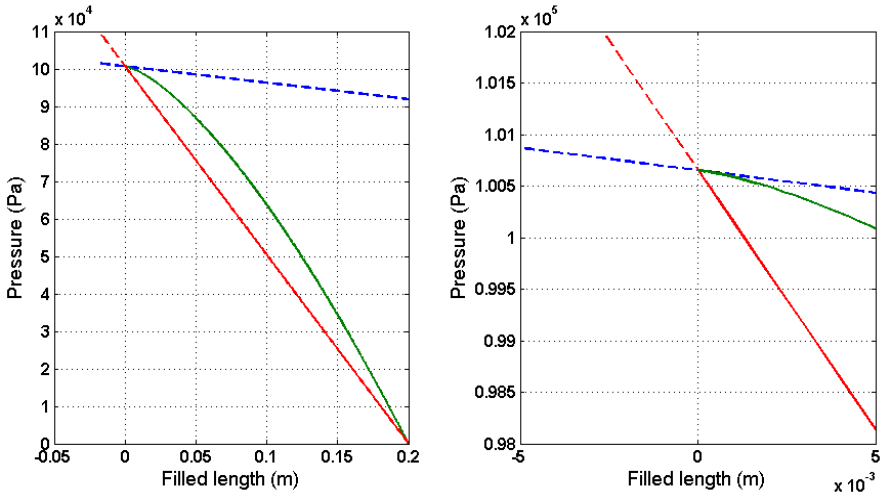

Figure 7. 12 - Pressure profiles and inlet pressure gradients of CSM experiments

From the figures it can be seen that comparing the calculated pressure gradients for the reduced inlet flow velocity with the pressure variation at the inlet of the VI experiments good correlation is obtained. This result supports the proposed inlet controlled filling behaviour.

To further interrogate the inlet pressure gradient, the numerical solution of the pressure profile at the inlet is further scrutinised. The first 4 numerical pressure solutions closest to the inlet are considered. These pressures occur within half a millimetre of the inlet or zero position. The numerical solution data points are shown in Figure 7.13 and 7.14. Utilising Microsoft Excel, a linear curve fit was plotted for the data points of the CSM and WR5 experiments. The linear fit was required to have a y intercept equal to that of inlet pressure. The gradient of the generated line is then equivalent to the inlet pressure gradient. The inlet pressures and plotted lines are shown in Figures 7.13 and 7.14. In addition the equations of the lines are also shown. The gradient of these lines correspond to the pressure gradient (dP/dx) occurring at the inlet of both experiments. The pressure gradients of CSM and WR5 calculated in this manner are 20320 and 43844 respectively. The magnitude of the pressure gradients (dP/dx) are consistent with the gradients predicted by the reduced inlet velocity which were 20438 and 43758.

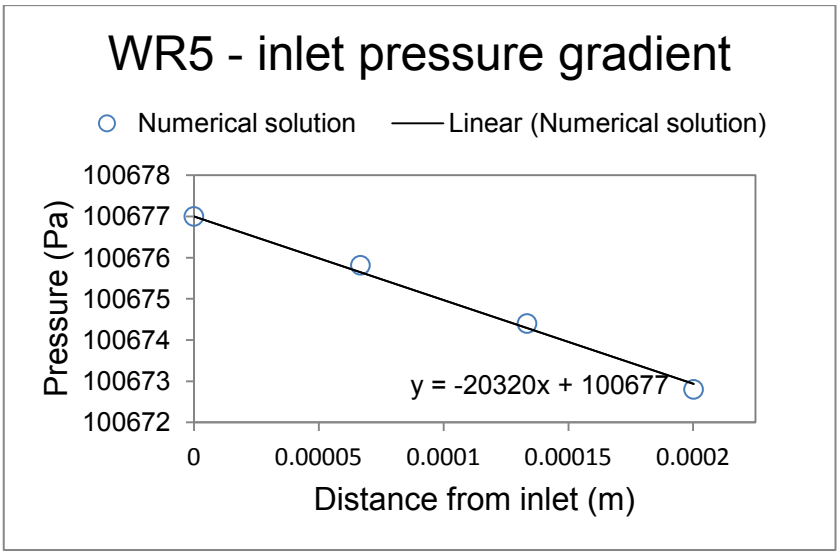

Figure 7. 13 - WR5 - inlet pressure gradient

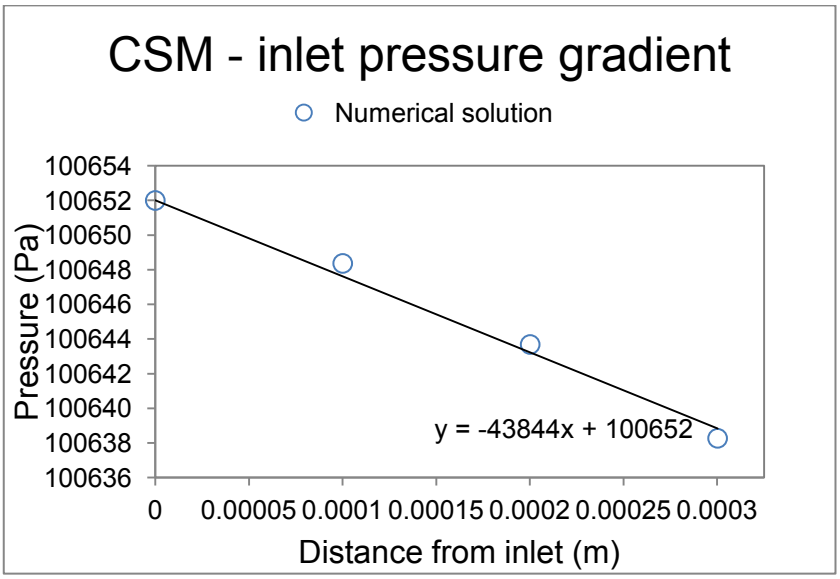

Figure 7. 14 - CSM - inlet pressure gradient

In summary, the inlet/entry or feed area affects the flow rate of VI. In a direct comparison between RTM and VI, a constant common inlet area is implemented. Due to pressure balancing between fluid and fabric, the inlet permeability is increased while the pressure gradient is significantly reduced. The resulting inlet velocity and therefore flow rate is then a combination of both the pressure gradient and permeability at the inlet.

During filling, the permeability at the inlet remains constant while the scalable pressure distribution controls the inlet pressure gradient. The pressure distribution and therefore inlet pressure gradient are scalable with filled length as in the RTM case. The result is

that the fill times are proportional to the square of the filled length which is also characteristic of RTM.

As the pressure balancing between the fluid and compacted preform is the key distinguishing factor between VI and RTM, longer fill times will always be observed in VI when comparing the processes under identical flow conditions.

7.4 Summary

Three fabric preforms are selected from the experimental work to evaluate three VI models. The experimental sets consisted of RTM and VI experiments performed on the same fabric preform. Using the results of each of the experiment sets, permeability and material characterisation for each of the three preforms is derived (Section 5). The modelled behaviour is then used as input into three VI models. The models solutions are compared back to the original VI experiments with respect to pressure profile, preform thickness and fill time behaviour for each of the three preforms being evaluated.

For all the VI models, the pressure profile solutions showed reasonable agreement with experimental pressure measurements (Figures 7.1 – 7.3). In addition, the differences between the model solutions were marginal when compared with each other for each of the three preforms. All models including the non accumulation steady state model appear to predict the pressure distribution accurately. As the experimentation showed no significant accumulation in the VI experiments the non accumulation steady state model as highlighted as applicable to the VI process.

The solution of the non accumulation steady state model was used to calculate preform thicknesses behind the flow front. Comparing the thicknesses with thickness measurements from the VI experiments yields reasonable agreement (Figures 7.4 – 7.6). This illustrates and highlights the prominent relationship between fluid pressure and displacement and the applicability of the non accumulation based model.

Previously, the pressure gradient at the flow front was assumed to control the flow front propagation and fill time behaviour in VI. If the thickness and permeability are the same at the flow front in the VI and RTM cases then the VI process should flow faster. All models predicted a larger pressure gradient at the flow front when compared with the RTM case. However, from the direct experimental comparison it is observed that the VI flows slower. This invalidated the assumption that the flow front controls the filling behaviour. From the experimental observations it was proposed that the inlet rather than the flow front controls the dynamic flow rate and consequently the fill times in VI. The proposed behaviour was supported through the evaluation of two experiment sets CSM and WR5. Details of the proposed behaviour and evaluation were presented in Section 7.3.

8. Conclusion

Vacuum infusion (VI) and resin transfer moulding (RTM) are comparable Liquid composite moulding processes. Both processes utilise differential pressure to drive resin into a mould cavity containing a dry preform constructed of fibre reinforcement. The key difference between the two processes is the formation of the mould cavity. The RTM process implements two rigid surfaces to create the cavity while the cavity of the VI processes is formed between one rigid surface and a flexible membrane or vacuum bag. The flexible cavity in VI influences and differentiates resin flow behaviour between the two processes. Modelling flow in the two processes enables the velocity, pressure and flow direction of the resin to be predicted.

Resin flow in the RTM process is modelled using Darcy's law. However, flow in the VI is not accurately modelled due to the added complexity introduced as a result of the flexible mould cavity. The aim and objective of the research was to investigate fluid flow behaviour and modelling of both processes with particular attention to VI.

To investigate fluid flow models it is necessary to compare the modelled with experimental flow behaviour. The models of fluid flow require specific properties unique a particular fabric preform to be characterised. Darcy's law applied in the RTM process requires a value of permeability to be determined while in the VI models, permeability and thickness/fibre volume faction are both functions of compaction pressure which is related to the fluid pressure.

In addressing the research aims, a novel approach was developed for the direct comparison of fluid flow in the RTM and VI processes under identical flow parameters and conditions. The comparison isolates the effect of preform thickness variation as a contributing and differentiating factor effecting flow. Through the unique setup and testing procedure, specific fabric preforms were tested under both VI and RTM conditions. The setup allowed for flow models for RTM and in particular VI, to be evaluated against experiments

The experimentation allowed for a value of permeability to be determined for modelling the RTM process using Darcy's law. The application of Darcy's law in the RTM process is based on the non accumulation and quasi steady state criteria. The comparative experimentation also allowed material and permeability characterisation to

be performed for three selected preforms. The characterised behaviour was used to evaluate three VI models. Two of the models were accumulation based while the third was based on a non accumulation quasi steady state application of Darcy's law where permeability and fibre volume fraction are both functions of pressure. The solutions of the all flow models were compared back to the original corresponding VI experiments. The pressure distribution behind the flow front, fill time and thickness behaviours were evaluated.

The observations and findings were made from the testing regime. The findings are discussed in two parts; pressure profile/distribution behind the flow front and flow front propagation or fill time.

The pressure profile is the fluid pressure distributions at locations between the inlet and flow front. The pressure distribution varies as the flow front advances. For the RTM processes the expected linear and scalable pressure profile was observed. Therefore the application of Darcy's law appears to accurately model the pressure distribution. The pressure profile in the VI experiments also showed scalable behaviour however a curved pressure profile was noted. As theorised by the VI models the difference in pressure profiles is the direct result of pressure balancing resulting in thickness changes. This conclusion is supported as the experimental setup only allowed thickness change to distinguish the difference between fluid behaviour in the two processes. Marginal differences were noted between the solutions of each of the three VI models. However, all models including the non accumulation base model accurately predicted the shape and magnitude of the pressure profiles. Utilising the pressure solution and the model for thickness/fibre volume fraction, the thickness behind the flow front was also predicted. The results compared well with the related experiments.

The fill time is the time taken for the flow front to reach a particular position within the mould cavity. In the rectilinear flow case of the present work this equates to a particular saturated or filled length. The fill times of the RTM experiments were in line with that predicted by Darcy's law. Permeability values were derived which represents a characteristic of a particular fabric preform for a given fibre volume fraction/porosity. The fill times of the VI experiments were noted to be longer than that of the equivalent RTM tests. The VI tests also revealed that the fill times are not only proportional to the square of the fill length, as in the RTM case, but also proportional to the square of the

mass present. In addition, the filled length in an RTM and corresponding VI experiment showed the same mass present during filling. This indicated that no significant accumulation occurred during the VI process. Therefore the slower flow front progression in VI must be the result of a slower mass flow rate entering the mould cavity for a particular filled length. Steady state flow experiments confirmed this behaviour. For a given filled length the mass flow rate entering the mould cavity is slower in VI than in the equivalent RTM process.

Previously, the authors who proposed the two accumulation based models for VI indicated that propagation of the flow front and therefore fill time was controlled by the conditions at the flow front. Then if the conditions at the flow from were the same for both an RTM and VI processes the steeper pressure gradient in VI will lead to faster flow front progression and shorter fill times. The experimental results contradict this interpretation. However both models do predict the pressure profile in VI.

The non accumulation VI model applies Darcy's law to VI in the same manner as in the RTM case. However, the pressure balancing leads to thickness variations which results in permeability and fibre volume fraction both being functions of pressure. A constant flow rate is maintained throughout a given filled length. The model is supported by the experiments showing no measurable accumulation in the VI process.

The flow rate entering the mould cavity in the VI process is less than the RTM case for a given filled length. The magnitude of the flow rate determines the flow front advancement and resulting fill times. Therefore a reduced flow rate in VI is responsible for differences between RTM and VI fill times. It is proposed in the present work that the flow rate in VI is controlled by the inlet and not the flow front as suggested by other authors. Evidence in support of this inlet controlled filling behaviour was found in the investigation of comparative tests. It was shown that a combination of the increase permeability and reduced pressure gradient at the inlet combine to determine the inlet velocity. This in turn results in a specific flow rate through the constant inlet/feed on entry area. The flow rate in VI however remains proportional to the filled length as in RTM. This effect results in a slower flow rate being established under VI for a given filled length. The reduced flow rate manifests as longer fill times in the direct comparison. As the pressure balancing between the fluid and compacted preform is the

key distinguishing factor between the two processes, longer fill times will be consistent under VI when directly compared with RTM under identical flow conditions.

The experimentation also revealed that other factors can influence flow behaviour in both moulding processes. Factors such as the inlet pipe dimensions and inlet configuration affect the flow rate in both processes equally. As the effect of these factors influence both RTM and VI equally the additional effects do not differentiate the flow behaviour. The key differentiating factor still remains the thickness variations resulting from the pressure balancing in VI.

The current study has identified two possible avenues of future research. Firstly, it would be advantageous to fully characterise and model the effect of the additional factors influencing flow other than the fabric preform. Secondly the testing equipment and procedure was designed to perform RTM and VI experiments in both line and point feed configurations. Point feed experiments could be performed and modelling of radial flow in the both processes could then be investigated.

References

[1] Handbook of Composite Fabrication. Shrewsbury, GBR: Smithers Rapra; 2001.

[2] Baker AA, Dutton S, Kelly D. Composite Materials for Aircraft Structures (2nd Edition). Reston, VA, USA: American Institute of Aeronautics and Astronautics; 2004.

[3] Tong L, Mouritz AP, Bannister MK. 3D Fibre Reinforced Polymer Composites. Kidlington, GBR: Elsevier Science & Technology; 2002.

[4] Modi D, Correia N, Johnson M, Long A, Rudd C, Robitaille F. Active control of the vacuum infusion process. Composites Part A: Applied Science and Manufacturing. 2007;38(5):1271-87.

[5] Comprehensive composite materials. Volume 2, Polymer matrix composites: Elsevier; 2001.

[6] Schubel PJ. Technical cost modelling for a generic 45-m wind turbine blade producedby vacuum infusion (VI). Renewable Energy. 2010;35(1):183-9.

[7] Wind energy and vacuum infusion. Reinforced Plastics. 2010;54(2):20.

[8] Kim D, Hennigan DJ, Beavers KD. Effect of fabrication processes on mechanical properties of glass fiber reinforced polymer composites for 49 meter (160 foot) recreational yachts. International Journal of naval architecture and ocean engineering. 2010;2(1):45-56.

[9] Acheson JA, Simacek P, Advani SG. The implications of fiber compaction and saturation on fully coupled VARTM simulation. Composites Part A: Applied Science and Manufacturing. 2004;35(2):159-69.

[10] Correia NC, Robitaille F, Long AC, Rudd CD, Šimáček P, Advani SG. Analysis of the vacuum infusion moulding process: I. Analytical formulation. Composites Part A: Applied Science and Manufacturing. 2005;36(12):1645-56.

[11] Correia N, Robitaille F, Long A, Rudd C, Šimá ek P, Advani SG. Use of resin transfer molding simulation to predict flow, saturation, and compaction in the VARTM process. Journal of fluids engineering. 2004;126:210.

[12] Williams C, Summerscales J, Grove S. Resin Infusion under Flexible Tooling (RIFT): a review. Composites Part A: Applied Science and Manufacturing. 1996;27(7):517-24.

[13] Simacek P, Eksik Ö, Heider D, Gillespie Jr JW, Advani S. Experimental Validation of Post-Filling Flow in Vacuum Assisted Resin Transfer Molding Processes. Composites Part A: Applied Science and Manufacturing. (Composites: Part A (2011), doi:10.1016/j.compositesa.2011.10.002).

[14] Darcy H, Brown GO, Garbrecht JD, Hager WH, Environmental, Institute WR. Henry P.G. Darcy and Other Pioneers in Hydraulics: Contributions in Celebration of the 200th Birthday of Henry Philibert Gaspard Darcy, June 23-26, 2003, Philadelphia, Pa: American Society of Civil Engineers; 2003.

[15] Terzaghi K, Peck RB, Mesri G. Soil mechanics in engineering practice. 3rd ed ed. New York: Wiley; 1996.

[16] Jing L. Development of integrated process design enviroment and statistical analysis of RTM process. Florida, USA: Florida State University; 2003.

[17] Versteeg HK. An introduction to computational fluid dynamics : the finite volume method: Longman Scientific & Technical; 1995.

[18] Zienkiewicz OC. The finite element method. Volume 3, Fluid dynamics: Butterworth-Heinemann,; 2000.

[19] Gupta V, Gupta SK. Fluid mechanics and its applications. New Delhi: New Age; 1984.

[20] Henderson FM. Open channel flow: Macmillan; 1966.

[21] Arbter R, Beraud JM, Binetruy C, Bizet L, Bréard J, Comas-Cardona S, et al. Experimental determination of the permeability of textiles: A benchmark exercise. Composites Part A: Applied Science and Manufacturing. 2011;42(9):1157-68.

[22] Koefoed MS. Modeling and simulation of the VARTM process for wind turbine blades: Aalborg university; 2003.

[23] Astrom B, Pipes RB. and Advani, SG. On flow through aligned fiber beds and it's application to composite processing. Journal of Composite Materials. 1992;26(9):1351-73.

[24] Pillai KM. Governing equations for unsaturated flow through woven fiber mats. Part 1. Isothermal flows. Composites Part A: Applied Science and Manufacturing. 2002;33(7):1007-19.

[25] Bruschke MV, Advani SG. A finite element/control volume approach to mold filling in anisotropic porous media. Polymer composites. 1990;11(6):398-405.

[26] Modi D. Modelling and active control of the vacuum infusion process for composite manufacture Nottingham, UK: University of Nottingham 2008.

[27] Modi D, Johnson M, Long A, Rudd C. Analysis of pressure profile and flow progression in the vacuum infusion process. Composites Science and Technology. 2009;69(9):1458-64.

[28] Ragondet A. Experimental characterisation of the vacuum infusion process. Nottingham, UK: University of Nottingham; 2005.

[29] Deléglise M, Binétruy C, Krawczak P. Solution to filling time prediction issues for constant pressure driven injection in RTM. Composites Part A: Applied Science and Manufacturing. 2005;36(3):339-44.

[30] Kang MK, Lee WI, Hahn HT. Analysis of vacuum bag resin transfer molding process. Composites Part A: Applied Science and Manufacturing. 2001;32(11):1553-60.

[31] Timms J, Bickerton S, Kelly PA. Laminate thickness and resin pressure evolution during axisymmetric liquid composite moulding with flexible tooling. Compos Part a-Appl S. 2012;43(4):621-30.

[32] Walbran WA, Verleye B, Bickerton S, Kelly PA. Prediction and experimental verification of normal stress distributions on mould tools during Liquid Composite Moulding. Composites Part A: Applied Science and Manufacturing. 2012;43(1):138-49.

[33] Govignon Q, Bickerton S, Morris J, Kelly PA. Full field monitoring of the resin flow and laminate properties during the resin infusion process. Composites Part A: Applied Science and Manufacturing. 2008;39(9):1412-26.

[34] Joubaud L, Achim V, Trochu F. Numerical simulation of resin infusion and reinforcement consolidation under flexible cover. Polymer composites. 2005;26(4):417-27.

[35] Yenilmez B, Senan M, Murat Sozer E. Variation of part thickness and compaction pressure in vacuum infusion process. Composites Science and Technology. 2009;69(11-12):1710-9.

[36] Kessels JFA, Jonker AS, Akkerman R. Fully flow modeling of resin infusion under flexible tooling using unstructured meshes and wet and dry compaction properties. Composites Part A: Applied Science and Manufacturing. 2007;38(1):51-60.

[37] Lawrence JM, Simacek P, Frey P, Bhat P, Gebauer T, Advani SG. The Compaction Behavior of Fibrous Preform Materials during the VARTM Infusion. AIP Conference Proceedings. 2007;907(1):1039-45.

[38] Andersson HM, Lundström TS, Gebart BR. Numerical model for vacuum infusion manufacturing of polymer composites. International Journal of Numerical Methods for Heat & Fluid Flow. 2003;13(3):383-94.

[39] Hammami A, Gebart B. Analysis of the vacuum infusion molding process. Polymer composites. 2000;21(1):28-40.

[40] Han K, Jiang S, Zhang C, Wang B. Flow modeling and simulation of SCRIMP for composites manufacturing. Composites Part A: Applied Science and Manufacturing. 2000;31(1):79-86.

[41] Chen B, Chou T-W. Compaction of woven-fabric preforms in liquid composite molding processes: single-layer deformation. Composites Science and Technology. 1999;59(10):1519-26.

[42] Chen B, Chou T-W. Compaction of woven-fabric preforms: nesting and multi-layer deformation. Composites Science and Technology. 2000;60(12-13):2223-31.

[43] Bickerton S, Buntain MJ, Somashekar AA. The viscoelastic compression behavior of liquid composite molding preforms. Composites Part A: Applied Science and Manufacturing. 2003;34(5):431-44.

[44] Kelly PA, Umer R, Bickerton S. Viscoelastic response of dry and wet fibrous materials during infusion processes. Composites Part A: Applied Science and Manufacturing. 2006;37(6):868-73.

[45] Saunders RA, Lekakou C, Bader MG. Compression in the processing of polymer composites 2. Modelling of the viscoelastic compression of resin-impregnated fibre networks. Composites Science and Technology. 1999;59(10):1483-94.

[46] Somashekar AA, Bickerton S, Bhattacharyya D. Compression deformation of a biaxial stitched glass fibre reinforcement: Visualisation and image analysis using X-ray micro-CT. Composites Part A: Applied Science and Manufacturing. 2011;42(2):140-50.

[47] Somashekar AA, Bickerton S, Bhattacharyya D. Exploring the non-elastic compression deformation of dry glass fibre reinforcements. Composites Science and Technology. 2007;67(2):183-200.

[48] Yenilmez B, Sozer EM. Compaction of e-glass fabric preforms in the Vacuum Infusion Process, A: Characterization experiments. Composites Part A: Applied Science and Manufacturing. 2009;40(4):499-510.

[49] Govignon Q, Bickerton S, Kelly PA. Simulation of the reinforcement compaction and resin flow during the complete resin infusion process. Composites Part A: Applied Science and Manufacturing. 2010;41(1):45-57.

[50] Song X. Vacuum assisted resin transfer molding (VARTM): Model development and Verification Blacksburg, Virginia, US: Virgina Polytechnic Institute 2003.

[51] Robitaille F, Gauvin R. Compaction of textile reinforcements for composites manufacturing. I: Review of experimental results. Polymer composites. 1998;19(2):198-216.

[52] Robitaille F, Gauvin R. Compaction of textile reinforcements for composites manufacturing. III: Reorganization of the fiber network. Polymer composites. 1999;20(1):48-61.

[53] Civan F. Porous Media Transport Phenomena. Hoboken NJ, USA: Wiley; 2011.

[54] Bayldon JM, Daniel IM. Flow modeling of the VARTM process including progressive saturation effects. Composites Part A: Applied Science and Manufacturing. 2009;40(8):1044-52.

[55] Gilat A, Subramaniam V. Numerical methods for engineers and scientists : an introduction with applications using MATLAB. Hoboken, N.J.: Wiley; 2008.

[56] Yang WY. Applied numerical methods using MATLAB. Hoboken, N.J.: Wiley-Interscience; 2005.

Appendix A

Derivation of the Correia vacuum infusion flow model [10]

Continuity equation Eq.2.10

$$\frac{\partial h}{\partial t} = -\frac{\partial (uh)}{\partial x} \qquad (A1)$$

Substituting Dary's law (eq2.1) for velocity (u) yields Eq. A2

$$\frac{\partial h}{\partial t} = -\frac{\partial}{\partial x}\left(\frac{-Kh}{\mu}\frac{\partial P}{\partial x}\right) \qquad (A2)$$

Viscosity remains constant

$$\frac{\partial h}{\partial t} = -\frac{1}{\mu}\frac{\partial}{\partial x}\left(-Kh\frac{\partial P}{\partial x}\right) \qquad (A3)$$

Cancelling the negative signs

$$\frac{\partial h}{\partial t} = \frac{1}{\mu}\frac{\partial}{\partial x}\left(Kh\frac{\partial P}{\partial x}\right) \qquad (A4)$$

Expanding partial differential – Both K and h are both functions of pressure

$$\frac{\partial h}{\partial t} = \frac{1}{\mu}\left[\left(\frac{\partial K}{\partial P}\frac{\partial P}{\partial x}h\frac{\partial P}{\partial x}\right) + \left(K\frac{\partial h}{\partial P}\frac{\partial P}{\partial x}\frac{\partial P}{\partial x}\right) + \left(Kh\frac{\partial P}{\partial x}\frac{\partial x}{\partial P}\frac{\partial P}{\partial x}\right)\right] \qquad (A5)$$

$$\frac{\partial h}{\partial t} = \frac{1}{\mu}\left[\left(h\frac{\partial K}{\partial P}\left(\frac{\partial P}{\partial x}\right)^2\right) + \left(K\frac{\partial h}{\partial P}\left(\frac{\partial P}{\partial x}\right)^2\right) + \left(Kh\frac{\partial^2 P}{\partial x^2}\right)\right] \qquad (A6)$$

Introducing a non dimensional parameter (α). *See figure 2.5*

$$\alpha = \frac{x}{L} \qquad (A7)$$

Where:

L - instantaneous flow front position or filled length

x – Distance between inlet ($\alpha = 0$) and flow front ($\alpha = 1$)

$$x = \alpha . L \qquad (A8)$$

$$\frac{\partial x}{\partial \alpha} = L \qquad (A9)$$

$$\partial x = \partial \alpha . L \qquad (A10)$$

Then, Substituting Eq.A10 into Eq. A6 yields Eq. A11

$$\frac{\partial h}{\partial t} = \frac{1}{\mu}\left[\left(h\frac{\partial K}{\partial P}\left(\frac{\partial P}{\partial \alpha . L}\right)^2\right) + \left(K\,\frac{\partial h}{\partial P}\left(\frac{\partial P}{\partial \alpha . L}\right)^2\right) + \left(Kh\,\frac{\partial^2 P}{(\partial \alpha . L)^2}\right)\right] \qquad (A11)$$

Expanding the square root term

$$\frac{\partial h}{\partial t} = \frac{1}{\mu}\left[\left(h\frac{\partial K}{\partial P}\left(\frac{\partial P^2}{\partial \alpha^2 . L^2}\right)\right) + \left(K\,\frac{\partial h}{\partial P}\left(\frac{\partial P^2}{\partial \alpha^2 . L^2}\right)\right) + \left(Kh\,\frac{\partial^2 P}{\partial \alpha^2 . L^2}\right)\right] \qquad (A12)$$

Extracting L^2 as a common factor

$$\frac{\partial h}{\partial t} = \frac{1}{\mu L^2}\left[\left(h\frac{\partial K}{\partial P}\left(\frac{\partial P^2}{\partial \alpha^2}\right)\right) + \left(K\,\frac{\partial h}{\partial P}\left(\frac{\partial P^2}{\partial \alpha^2}\right)\right) + \left(Kh\,\frac{\partial^2 P}{\partial \alpha^2}\right)\right] \qquad (A13)$$

Rewriting yields

$$\frac{\partial h}{\partial t} = \frac{1}{\mu L^2}\left[\left(h\frac{\partial K}{\partial P}\left(\frac{\partial P}{\partial \alpha}\right)^2\right) + \left(K\,\frac{\partial h}{\partial P}\left(\frac{\partial P}{\partial \alpha}\right)^2\right) + \left(Kh\,\frac{\partial^2 P}{\partial \alpha^2}\right)\right] \qquad (A14)$$

Remove K and h from the square brackets yields

$$\frac{\partial h}{\partial t} = \frac{Kh}{\mu L^2}\left[\left(\frac{1}{K}\frac{\partial K}{\partial P}\left(\frac{\partial P}{\partial \alpha}\right)^2\right) + \left(\frac{1}{h}\,\frac{\partial h}{\partial P}\left(\frac{\partial P}{\partial \alpha}\right)^2\right) + \left(\frac{\partial^2 P}{\partial \alpha^2}\right)\right] \qquad (A15)$$

Simplifying yields eq A16

$$\frac{\partial h}{\partial t} = \frac{Kh}{\mu L^2}\left[\left(\frac{1}{K}\frac{\partial K}{\partial P} + \frac{1}{h}\,\frac{\partial h}{\partial P}\right)\left(\frac{\partial P}{\partial \alpha}\right)^2 + \left(\frac{\partial^2 P}{\partial \alpha^2}\right)\right] \qquad (A16)$$

Now considering the LHS of Eq. A16, with reference to figure 2.5

$$\frac{\partial h}{\partial t} = \frac{\partial h}{\partial P}\,\frac{\partial P}{\partial \alpha}\,\frac{\partial \alpha}{\partial L}\,\frac{\partial L}{\partial t} \qquad (A17)$$

Calculating $(\partial \alpha/\partial L)$ from Eq. A7

$$\alpha = \frac{x}{L}$$

$$\frac{\partial \alpha}{\partial L} = -\frac{x}{L^2} \qquad (A18)$$

Calculating $(\partial L/\partial t)$

Implementing a constant flow rate assumption:

$$Q_x = Q_{ff}$$

Where Q_x = flow rate at a position behind the flow front

Q_{ff} = Flow rate at the flow front

$$A_1 V_1 = A_{ff} V_{ff}$$

$$b_1 h_1 V_1 = b_{ff} h_{ff} V_{ff}$$

But width (b) is constant - Then

$$h_1 V_1 = h_{ff} V_{ff}$$

Or

$$h_1 u_1 = h_{ff} u_{ff}$$

But

Flow front velocity

$$u_{ff} = \frac{\partial L}{\partial t}$$

Then

$$h_1 u_1 = h_{ff} \frac{\partial L}{\partial t}$$

$$\frac{h_1}{h_{ff}} u_1 = \frac{\partial L}{\partial t}$$

Let

$$\frac{h_1}{h_{ff}} = h^*$$

then

$$\frac{\partial L}{\partial t} = u_1 h^*$$

Substituting Darcy's law

$$\frac{\partial L}{\partial t} = -\frac{K}{\mu}\frac{\partial P}{\partial x}h^*$$

$$\frac{\partial L}{\partial t} = -\frac{K}{\mu}\frac{\partial P}{\partial x}h^*$$

$$\frac{\partial L}{\partial t} = -\frac{Kh^*}{\mu}\frac{\partial P}{\partial \alpha}\frac{\partial \alpha}{\partial x} \qquad (A19)$$

Sub Eq. (A18, A19) into Eq. A17 yields Eq.A20

$$\frac{\partial h}{\partial t} = \frac{\partial h}{\partial P}\frac{\partial P}{\partial \alpha}\frac{\partial \alpha}{\partial L}\frac{\partial L}{\partial t} \qquad (A17)$$

$$\frac{\partial h}{\partial t} = \left(\frac{\partial h}{\partial P}\frac{\partial P}{\partial \alpha}\right)\left(-\frac{x}{L^2}\right)\left(-\frac{Kh^*}{\mu}\frac{\partial P}{\partial \alpha}\frac{\partial \alpha}{\partial x}\right) \qquad (A20)$$

Rewriting and cancelling negative signs

$$\frac{\partial h}{\partial t} = \left(\frac{1}{L^2}\right)\left(\frac{\partial h}{\partial P}\right)\left(x.\frac{\partial \alpha}{\partial x}\right)\left(\frac{Kh^*}{\mu}\right)\left(\frac{\partial P}{\partial \alpha}\right)^2 \qquad (A21)$$

But from Eq. A7 $\frac{\partial \alpha}{\partial x} = \frac{1}{L}$ – then:

$$\frac{\partial h}{\partial t} = \left(\frac{1}{L^2}\right)\left(\frac{\partial h}{\partial P}\right)\left(\frac{x}{L}\right)\left(\frac{Kh^*}{\mu}\right)\left(\frac{\partial P}{\partial \alpha}\right)^2 \qquad (A22)$$

But from Eq. A7 $\frac{x}{L} = \alpha$ – then:

$$\frac{\partial h}{\partial t} = \left(\frac{1}{L^2}\right)\left(\frac{\partial h}{\partial P}\right)(\alpha)\left(\frac{Kh^*}{\mu}\right)\left(\frac{\partial P}{\partial \alpha}\right)^2 \qquad (A23)$$

Simplifying yields Eq. A24

$$\frac{\partial h}{\partial t} = \left(\frac{\alpha}{L^2}\right)\left(\frac{\partial h}{\partial P}\right)\left(\frac{Kh^*}{\mu}\right)\left(\frac{\partial P}{\partial \alpha}\right)^2$$

$$\frac{\partial h}{\partial t} = \frac{Kh^*\alpha}{\mu L^2}\left(\frac{\partial h}{\partial P}\right)\left(\frac{\partial P}{\partial \alpha}\right)^2 \qquad (A24)$$

Substituting Eq. A24 For the LHS of Eq. A16 yields:

$$\frac{Kh^*\alpha}{\mu L^2}\left(\frac{\partial h}{\partial P}\right)\left(\frac{\partial P}{\partial \alpha}\right)^2 = \frac{Kh}{\mu L^2}\left[\left(\frac{1}{K}\frac{\partial K}{\partial P} + \frac{1}{h}\frac{\partial h}{\partial P}\right)\left(\frac{\partial P}{\partial \alpha}\right)^2 + \left(\frac{\partial^2 P}{\partial \alpha^2}\right)\right] \qquad (A25)$$

Simplification and rewriting of Eq. A25 yields Eq. A26.

Eq A26 isthe vacuum infusion flow model proposed by Corriea.

$$h^*\alpha\left(\frac{\partial h}{\partial P}\right)\left(\frac{\partial P}{\partial \alpha}\right)^2 = h\left[\left(\frac{1}{K}\frac{\partial K}{\partial P} + \frac{1}{h}\frac{\partial h}{\partial P}\right)\left(\frac{\partial P}{\partial \alpha}\right)^2 + \left(\frac{\partial^2 P}{\partial \alpha^2}\right)\right]$$

$$\frac{h^*\alpha}{h}\left(\frac{\partial h}{\partial P}\right)\left(\frac{\partial P}{\partial \alpha}\right)^2 = \left(\frac{1}{K}\frac{\partial K}{\partial P} + \frac{1}{h}\frac{\partial h}{\partial P}\right)\left(\frac{\partial P}{\partial \alpha}\right)^2 + \left(\frac{\partial^2 P}{\partial \alpha^2}\right)$$

$$\frac{h^*\alpha}{h}\frac{\partial h}{\partial P}\left(\frac{\partial P}{\partial \alpha}\right)^2 = \frac{1}{K}\frac{\partial K}{\partial P}\left(\frac{\partial P}{\partial \alpha}\right)^2 + \frac{1}{h}\frac{\partial h}{\partial P}\left(\frac{\partial P}{\partial \alpha}\right)^2 + \left(\frac{\partial^2 P}{\partial \alpha^2}\right)$$

$$-\frac{\partial^2 P}{\partial \alpha^2} = \frac{1}{K}\frac{\partial K}{\partial P}\left(\frac{\partial P}{\partial \alpha}\right)^2 + \frac{1}{h}\frac{\partial h}{\partial P}\left(\frac{\partial P}{\partial \alpha}\right)^2 - \frac{h^*\alpha}{h}\frac{\partial h}{\partial P}\left(\frac{\partial P}{\partial \alpha}\right)^2$$

$$\frac{\partial^2 P}{\partial \alpha^2} = -\frac{1}{K}\frac{\partial K}{\partial P}\left(\frac{\partial P}{\partial \alpha}\right)^2 + \frac{(h^*\alpha - 1)}{h}\frac{\partial h}{\partial P}\left(\frac{\partial P}{\partial \alpha}\right)^2$$

$$\frac{d^2 P}{d\alpha^2} = -\left[\left(\frac{1 - h^*\alpha}{h}\right)\frac{dh}{dP} + \left(\frac{1}{K}\right)\frac{dK}{dP}\right]\left(\frac{dP}{d\alpha}\right)^2 \qquad (A26)$$

Appendix B

Derivation of the Modi vacuum infusion flow model [26]

Note: The flow model formulated by Modi is identical to the Corriea formulation (Appendix A) up to equation A16. Departure from the Correia model is in how the left hand term of Eq. A16 is presented. More specifically the term expressing the change in filled length with time ($\partial L/\partial t$).

Continuing from eq A17 of Appendix A and considering the LHS of Eq. A16.

$$\frac{\partial h}{\partial t} = \frac{\partial h}{\partial P}\frac{\partial P}{\partial \alpha}\frac{\partial \alpha}{\partial L}\frac{\partial L}{\partial t} \qquad (A17)$$

Calculating ($\partial \alpha/\partial L$) from Eq.A7

$$\alpha = \frac{x}{L}$$

$$\frac{\partial \alpha}{\partial L} = -\frac{x}{L^2} \qquad (A18)$$

Expression for the change in fill length with time. ($\partial L/\partial t$)

$$\frac{\partial L}{\partial t} = -\frac{K}{\mu \phi}\frac{\partial P}{\partial \alpha}\frac{\partial \alpha}{\partial L} \qquad (B1)$$

Substituting Eq.B1 and Eq. A18 into Eq. A17 yields Eq. B2

$$\frac{\partial h}{\partial t} = \frac{\partial h}{\partial P}\frac{\partial P}{\partial \alpha}\frac{\partial \alpha}{\partial L}\left(-\frac{K}{\mu\phi}\frac{\partial P}{\partial \alpha}\frac{\partial \alpha}{\partial L}\right) \quad (B2)$$

simplifying

$$\frac{\partial h}{\partial t} = -\frac{K}{\mu\phi}\left(\frac{\partial \alpha}{\partial L}\right)^2\frac{\partial h}{\partial P}\left(\frac{\partial P}{\partial \alpha}\right)^2$$

but

$$\frac{\partial \alpha}{\partial L} = -\frac{\alpha}{L}$$

then

$$\frac{\partial h}{\partial t} = -\frac{K}{\mu\phi}\left(-\frac{\alpha}{L}\right)^2\frac{\partial h}{\partial P}\left(\frac{\partial P}{\partial \alpha}\right)^2$$

Simplifying yields Eq. B3

$$\frac{\partial h}{\partial t} = \frac{K\alpha^2}{\mu\phi L^2}\frac{\partial h}{\partial P}\left(\frac{\partial P}{\partial \alpha}\right)^2 \quad (B3)$$

Substituting Eq. B3 for the LHS of Eq. A16 yields Eq.B4

$$\frac{K\alpha^2}{\mu\phi L^2}\frac{\partial h}{\partial P}\left(\frac{\partial P}{\partial \alpha}\right)^2 = \frac{Kh}{\mu L^2}\left[\left(\frac{1}{K}\frac{\partial K}{\partial P}+\frac{1}{h}\frac{\partial h}{\partial P}\right)\left(\frac{\partial P}{\partial \alpha}\right)^2+\left(\frac{\partial^2 P}{\partial \alpha^2}\right)\right] \quad (B4)$$

Manipulation of Eq. B4 yields Eq. B5. Which is the vacuum infusion flow model by Modi.

$$\frac{\alpha^2}{\phi}\frac{\partial h}{\partial P}\left(\frac{\partial P}{\partial \alpha}\right)^2 = h\left[\left(\frac{1}{K}\frac{\partial K}{\partial P}+\frac{1}{h}\frac{\partial h}{\partial P}\right)\left(\frac{\partial P}{\partial \alpha}\right)^2+\left(\frac{\partial^2 P}{\partial \alpha^2}\right)\right]$$

$$\frac{\alpha^2}{h\phi}\frac{\partial h}{\partial P}\left(\frac{\partial P}{\partial \alpha}\right)^2 = \left[\left(\frac{1}{K}\frac{\partial K}{\partial P} + \frac{1}{h}\frac{\partial h}{\partial P}\right)\left(\frac{\partial P}{\partial \alpha}\right)^2 + \left(\frac{\partial^2 P}{\partial \alpha^2}\right)\right]$$

Expanding the RHS

$$\frac{\alpha^2}{h\phi}\frac{\partial h}{\partial P}\left(\frac{\partial P}{\partial \alpha}\right)^2 = \left[\left(\frac{1}{K}\frac{\partial K}{\partial P}\left(\frac{\partial P}{\partial \alpha}\right)^2 + \frac{1}{h}\frac{\partial h}{\partial P}\left(\frac{\partial P}{\partial \alpha}\right)^2\right) + \left(\frac{\partial^2 P}{\partial \alpha^2}\right)\right]$$

$$\frac{\alpha^2}{h\phi}\frac{\partial h}{\partial P}\left(\frac{\partial P}{\partial \alpha}\right)^2 = \frac{1}{K}\frac{\partial K}{\partial P}\left(\frac{\partial P}{\partial \alpha}\right)^2 + \frac{1}{h}\frac{\partial h}{\partial P}\left(\frac{\partial P}{\partial \alpha}\right)^2 + \left(\frac{\partial^2 P}{\partial \alpha^2}\right)$$

Rearranging

$$-\left(\frac{\partial^2 P}{\partial \alpha^2}\right) = \frac{1}{h}\frac{\partial h}{\partial P}\left(\frac{\partial P}{\partial \alpha}\right)^2 - \frac{\alpha^2}{h\phi}\frac{\partial h}{\partial P}\left(\frac{\partial P}{\partial \alpha}\right)^2 + \frac{1}{K}\frac{\partial K}{\partial P}\left(\frac{\partial P}{\partial \alpha}\right)^2$$

$$\left(\frac{\partial^2 P}{\partial \alpha^2}\right) = -\frac{1}{h}\frac{\partial h}{\partial P}\left(\frac{\partial P}{\partial \alpha}\right)^2 + \frac{\alpha^2}{h\phi}\frac{\partial h}{\partial P}\left(\frac{\partial P}{\partial \alpha}\right)^2 - \frac{1}{K}\frac{\partial K}{\partial P}\left(\frac{\partial P}{\partial \alpha}\right)^2$$

Grouping like terms

$$\left(\frac{\partial^2 P}{\partial \alpha^2}\right) = -\left(\frac{1}{h} + \frac{\alpha^2}{h\phi}\right)\frac{\partial h}{\partial P}\left(\frac{\partial P}{\partial \alpha}\right)^2 - \frac{1}{K}\frac{\partial K}{\partial P}\left(\frac{\partial P}{\partial \alpha}\right)^2$$

$$\left(\frac{\partial^2 P}{\partial \alpha^2}\right) = -\left(\frac{\phi + \alpha^2}{h\phi}\right)\frac{\partial h}{\partial P}\left(\frac{\partial P}{\partial \alpha}\right)^2 - \frac{1}{K}\frac{\partial K}{\partial P}\left(\frac{\partial P}{\partial \alpha}\right)^2$$

$$\left(\frac{\partial^2 P}{\partial \alpha^2}\right) = -\left(\frac{\phi + \alpha^2}{h\phi}\right)\frac{\partial h}{\partial P}\left(\frac{\partial P}{\partial \alpha}\right)^2 - \frac{1}{K}\frac{\partial K}{\partial P}\left(\frac{\partial P}{\partial \alpha}\right)^2$$

$$\frac{d^2 P}{d\alpha^2} = -\left[\left(\frac{\phi + \alpha^2}{h\phi}\right)\frac{dh}{dP} + \left(\frac{1}{K}\right)\frac{dK}{dP}\right]\left(\frac{dP}{d\alpha}\right)^2 \qquad (B5)$$